The finite element approximation of Semi-linear Elliptic PDEs with Critical Exponents in the Cube

C.J. Budd[‡], A.R. Humphries[§] and A.J. Wathen[¶]

November 5, 1996

Abstract

We consider the finite element solution of the parameterised semi-linear elliptic equation $\Delta u + \lambda u + u^5 = 0, u > 0$, where u is defined in the unit cube and is zero on the boundary of the cube. This equation is important in analysis and it is known that there is a value $\lambda_0 > 0$ such that no solutions exist for $\lambda < \lambda_0$. By solving a related linear equation we obtain an upper bound for λ_0 which is also conjectured to be an estimate for its value. We then present results on computations on the full nonlinear problem. Using formal asymptotic methods we derive an approximate description of u which is supported by the numerical calculations. The asymptotic methods also give sharp estimates both for the error in the finite element solution when $\lambda > \lambda_0$ and for the form of the spurious numerical solutions which are known to exist when $\lambda < \lambda_0$. These estimates are then used to post-process the numerical results to obtain a sharp estimate for λ_0 which agrees with the conjectured value.

Keywords Semi-linear elliptic partial differential equation, finite element method, critical Sobolev exponent, spurious solutions, matched asymptotic expansion.

[‡]School of Mathematics, University of Bath, Claverton Down, Bath BA2 7AY, UK.

[§]Centre for Mathematical Analysis and its Applications, School of Mathematical Sciences, University of Sussex, Brighton, BN1 9QH, UK.

[¶]Oxford University Computing Laboratory, Wolfson Building, Parks Road, Oxford OX1 3QD, UK.

1 Introduction

1.1 Preliminaries

An interesting class of parametrised semi-linear elliptic partial differential equations with solutions which develop isolated singularities as the parameter varies, is given by the system

$$\left.\begin{array}{rl} \Delta u + \lambda u + u^5 = 0, & \text{on } \Omega \subset \mathbb{R}^3, \\ u > 0 & \text{in } \Omega, \\ u = 0 & \text{on } \partial\Omega. \end{array}\right\} \tag{1.1}$$

where Ω is a bounded domain in $\mathbb{R}^3$. For this problem there exist domains Ω and a parameter $\lambda_0 > 0$ such that $\|u\|_\infty \to \infty$ as $\lambda \to \lambda_0$ with no (positive) solution existing when $\lambda < \lambda_0$. Our studies focus on the finite element approximation of u close to this singularity, calculating λ_0 accurately and deriving sharp error estimates which also describe the behaviour of the numerical solutions when $\lambda < \lambda_0$.

The model problem (1.1) was introduced by Brezis and Nirenberg in the seminal paper [5], as a special case of the more general problem

$$\left.\begin{array}{rll} \Delta u + f(u;\lambda) = 0, & \text{on } \Omega \subset \mathbb{R}^n, & n \geqslant 3 \\ u > 0 & \text{in } \Omega, & \\ u = 0 & \text{on } \partial\Omega, & \end{array}\right\} \tag{1.2}$$

where the parametrised function $f(u;\lambda)$ has the property that as $u \to \infty$ there exists a strictly positive constant C such that

$$f(u;\lambda)u^{-p_c} \to C \quad \text{where } p_c \equiv \frac{n+2}{n-2}, \quad n \geqslant 3. \tag{1.3}$$

The value p_c is called the critical Sobolev exponent for $\mathbb{R}^n$, $n \geqslant 3$ and f is said to grow at a critical rate. The most subtle behaviour is observed in the case of three space dimensions so that $n = 3$ and $p_c = 5$; equation (1.1) falls within this class, and it is this case we will study in this paper.

The study of (1.1) and (1.2) was originally motivated by the *Yamabé problem* of constructing a manifold of a given curvature, which requires the solution of a critical problem related to (1.1) and (1.2) on a Riemannian manifold, it also has applications in the study of stellar structure. However the challenges posed by (1.1) and (1.2) are such that since the paper of Brezis and Nirenberg [5] these equations have been studied as problems in their own right and have provided a rich source of open and fascinating problems in analysis. The reason for this richness, is that if the function f grows more slowly than the critical rate, then variational techniques may be used in the analysis of (1.2), however these techniques break down for critically growing nonlinearities. This leads to delicate questions concerning the existence (in particular the value of λ_0 at which solutions cease to exist) the uniqueness and regularity of the solutions. The analytic investigations of the solution branch (λ, u) of (1.1) have mostly concentrated upon radially symmetric solutions in the sphere and these investigations have led to many conjectures about the behaviour in more general domains. The first purpose of this paper is to apply the finite element method to make a numerical study of the branch (λ, U_h) of discrete solutions of a weak form of (1.1) when Ω is the unit cube. For this investigation we consider piecewise trilinear functions defined on a uniform mesh of element size h. We give numerical evidence to support some outstanding conjectures on the value of λ_0, the uniqueness of the solution and the behaviour of the solution as it becomes more singular in the limit of $\lambda \to \lambda_0$.

As the finite element method is based upon variational ideas it inherits many of the interesting structures of the continous problem related to the breakdown of the variational method. Its application to solve (1.1) is consequently delicate and we need to introduce several new ideas to determine the solution accurately and to obtain good error estimates for $\|U_h - u\|_\infty$. Difficulties arise for two reasons. Firstly, both u and Δu become unbounded as λ approaches λ_0. Secondly, the linear differential operator L_λ derived by linearising (1.1) about the solution and defined by

$$L_\lambda \varphi = \Delta\varphi + \lambda\varphi + 5u^4\varphi, \quad \varphi|_{\partial\Omega} = 0 \tag{1.4}$$

is known to have an inverse which itself becomes unbounded in the L_∞ operator norm as $\lambda \to \lambda_0$ [7]. Estimates of the error $\|U_h - u\|_\infty$ in the solution of (1.1) are presented in [15],[13]. These are proportional to the product of $\|\Delta u\|_\infty$ and $\|L^{-1}\|_\infty$ and consequently are very large as $\lambda \to \lambda_0^+$. Furthermore, variational arguments prove that spurious numerical solutions of (1.1) exist when $\lambda \leqslant \lambda_0$. Unlike convergent solutions, the maximum norm of the spurious solutions grows without bound as $h \to 0$. However, we show that this growth is slow, being proportional to $h^{-1/4}$. The spurious solutions lie on the same continuous solution branch as those which converge to u under mesh refinement and are almost indistinguishable from them if λ_0 is unknown. Consequently the range of existence of the true solutions is hard to determine.

In Figure 1.1 we present a graph of the infinity norm of the discrete solution U_h as a function of λ and also indicate a value of $\lambda_0 = 7.5045$ which is conjectured from further computations in this paper. This graph was obtained for a solution of (1.1) on the unit cube $0 \leqslant x, y, z \leqslant 1$ using the finite element method with piecewise trilinear basis functions defined over cubes of side $h = 1/60, \ldots, 1/100$. Observe that each of the curves looks smooth with no significant hint of singular behaviour occuring close to λ_0.

In Figure 1.2 we present a cross section of the resulting solution taken in the plane $z = 1/2$ with $h = 1/100$ for $\lambda = (i)20, (ii)15, (iii)7.5045, (iv)0$. In this graph figure (i) and (ii) are approximations to true solutions, (iv) is certainly spurious and further computations strongly imply that (iii) is also spurious. From these figures we observe that each of these figures exhibits a peak forming in the centre of the cube which grows as λ is reduced. Although the peak in (iii) and (iv) is higher than those in (i) and (ii), its appearence does not appear to be significantly different (i.e. it appears well resolved by the mesh) and it is very hard a-priori to distinguish from numerical evidence alone between the true and spurious solutions.

As the singularity forms it is computationally impossible to use a fine enough uniform mesh to resolve its structure, and indeed the employment of a fixed mesh ultimately leads to the spurious solutions. Such considerations suggest that instead of using a uniform mesh, an adaptive approach should be taken which places a higher density of mesh points close to the singularity. Typically such methods places points where an a-priori estimate of the local truncation error [27] or an a-posteriori estimate of the solution error [3], is high. However, such methods are hard to implement in three dimensions and can also be misleading, as due to the unboundedness of $\|L_\lambda^{-1}\|_\infty$, the above error estimates for the solution are not sharp. Some preliminary computations of radially symmetric solutions of (1.1) reported in [8] demonstrate that adaptive methods based upon local truncation or a-posteriori error estimates are not particularly accurate and still admit spurious solutions, although these now look very smooth on the adapted meshes.

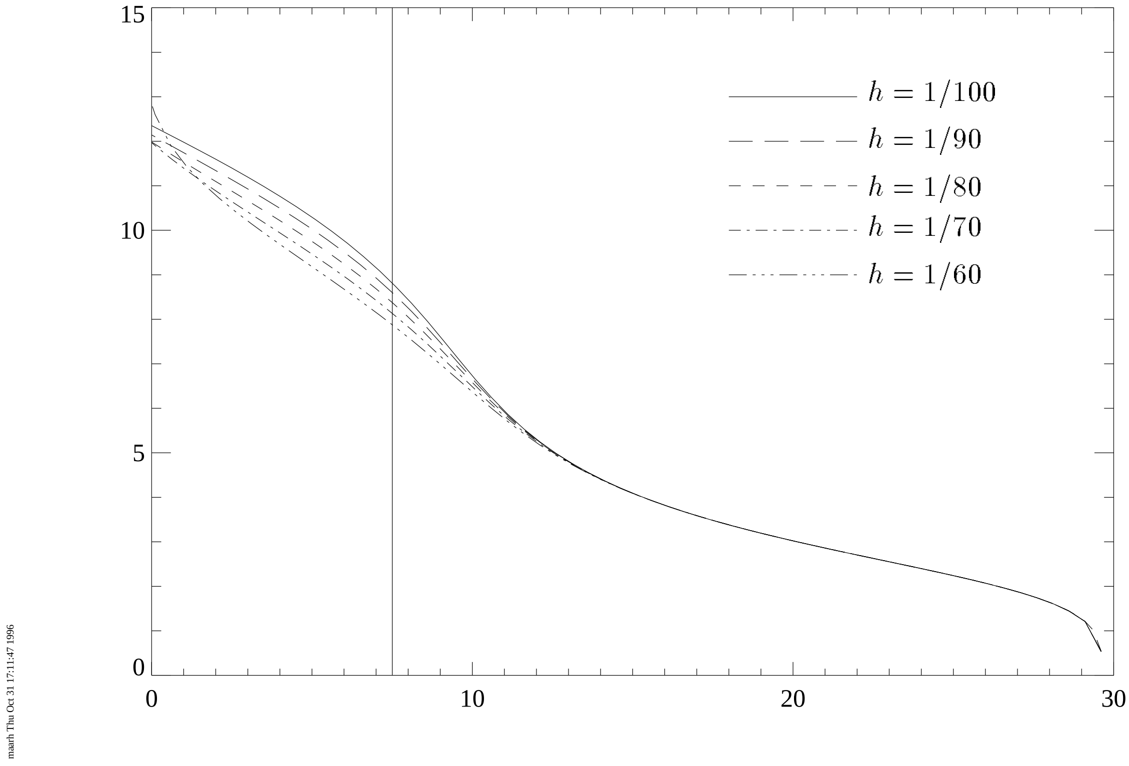

Figure 1.1: Graph of $\|U_h\|_\infty$ against λ, for grids varying between $h = 1/60$ and $h = 1/100$.

As a consequence, we adopt a different approach here by looking at the solution on a uniform mesh and use formal asymptotic methods, scaling arguments and an approximation result (in Lemma 6.1) to obtain sharp estimates of both the convergent and spurious solutions. By using sufficiently fine meshes these estimates are descriptive and can be used to post-process the numerical solution to give a much more accurate solution of (1.1) and an estimate of λ_0. We show that if λ is close to but greater than λ_0 then there is a constant C (which can be calculated a-priori) such that if h is sufficiently small (in particular if $h^2\|U_h\|_\infty^8$ is small) then

$$\frac{\left|\|u\|_\infty - \|U_h\|_\infty\right|}{\|U_h\|_\infty} \approx Ch^2\|U_h\|_\infty^8/(2\lambda). \tag{1.5}$$

If h satisfies the less restrictive requirement that $h^2\|U_h\|_\infty^4$ is small then

$$\|u\|_\infty \approx \|U_h\|_\infty / \sqrt{1 - Ch^2\|U_h\|^8/\lambda}, \tag{1.6}$$

which reduces to (1.5) in the limit of small h. In contrast, if $\lambda = \lambda_0$ so that the numerical solution is spurious we have that

$$\|U_h\|_\infty \approx \left(\frac{\lambda_0}{C}\right)^{1/8} h^{-1/4} \tag{1.7}$$

so that $\|U_h\|_\infty$ grows slowly as h decreases. We note that the value of C in the above depends upon the elements used but not upon the domain, so that these results have immediate extensions to problems with more complex geometries.

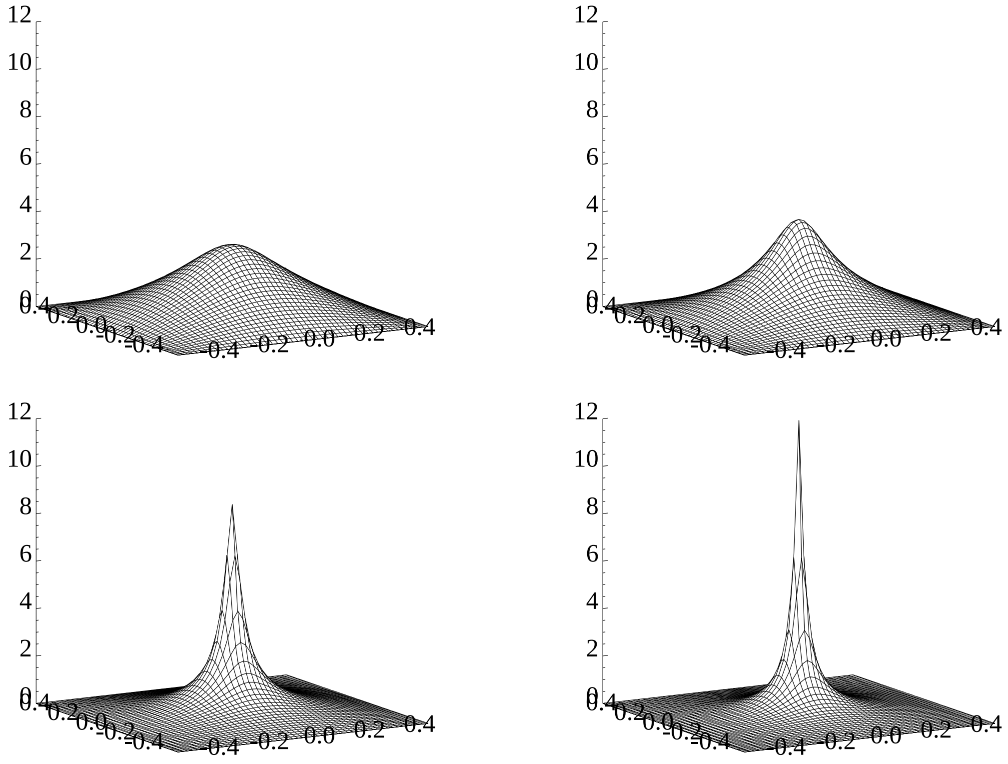

Figure 1.2: Cross section of the numerical solution U_h through centre of cube with $h = 1/100$ and (i) $\lambda = 20$, (ii) $\lambda = 15$, (iii) $\lambda = \lambda_{**} = 7.5045$, (iv) $\lambda = 0$.

Although the restriction that $h^2\|U_h\|_\infty^4$ be small means that we must use a moderately fine mesh for these results to be sharp when $\|U_h\|_\infty$ is large, the restriction is not too severe and we are able to perform computations with such meshes. The formula (1.6) then gives us a means of post-processing the results to obtain a more accurate value for $\|u\|_\infty$ and hence to estimate λ_0.

As an application of these methods we give computational evidence to support a conjecture made by McLeod [20], that λ_0 is equal to a value λ_{**} obtained by solving a related linear problem. (This is the value of λ indicated in Figure 1.1.) We also give strong evidence to show that the solutions in the cube are unique and have a high degree of radial symmetry away from the boundary.

The layout of the remainder of this paper is as follows. In Section 2 we give a brief summary of the significant analytic results and conjectures concerning (1.1) and in particular describe the form of the developing singularity. In Section 3 we derive the finite element method and state some known results on its convergence. In Section 4 we apply this method to solve a linear problem which approximates (1.1) when u is large. This gives both an upper bound and an estimate λ_{**} for λ_0. In Section 5 we compute solutions for the full problem (1.1) and present the results, indicating that for sufficiently fine meshes the solutions obey a scaling law. In Section 6 we apply formal asymptotic techniques to derive an improved description of both u and U_h. Finally, in Section 7, we use the asymptotic formula to derive the estimates (1.5),(1.6),(1.7) and then apply (1.6) to post-process the numerical results to obtain a more accurate description of the solution.

2 The qualitative form of the analytic solution branch

2.1 Existence

We define bilinear operators $a(u,v)$ and $\langle u,v\rangle$ by

$$a(u,v) = \int_\Omega \nabla u.\nabla v d\Omega \qquad \text{and} \qquad \langle u,v\rangle = \int_\Omega uv d\Omega,$$

and denote by $H_0^1(\Omega)$ the usual Sobolev space of functions vanishing on the boundary of Ω with norm defined by $\|u\|^2_{H_0^1} = a(u,u)$. Furthermore, let $\lambda_1(\Omega)$ be the smallest eigenvalue, with positive eigenfunction vanishing on the boundary of Ω, of the differential operator $-\Delta$. A weak solution $u \in H_0^1(\Omega)$, of the general problem

$$\left.\begin{array}{ll} \Delta u + \lambda u + u^p = 0, & \text{on } \Omega \subset \mathbb{R}^3, \\ u > 0 & \text{in } \Omega, \\ u = 0 & \text{on } \partial\Omega. \end{array}\right\} \tag{2.1}$$

is a zero of the function $\Psi : H_0^1(\Omega) \to H^{-1}(\Omega)$ defined by

$$\Psi(u)\varphi = -a(u,\varphi) + \langle \lambda u + u^p, \varphi\rangle \tag{2.2}$$

Equivalently, u is a critical point (typically a saddle-point) of the function $\Phi : H_0^1(\Omega) \to \mathbb{R}$ defined by

$$\Phi(u) = -\frac{1}{2}a(u,u) + \int_\Omega \left(\lambda\frac{u^2}{2} + \frac{u^{p+1}}{p+1}\right) d\Omega \tag{2.3}$$

If $\lambda < \lambda_1$ then, then by applying the Mountain Pass Theorem from the calculus of variations, it is shown (for example in [12]), that a sufficient condition for the existence of such a (non-trivial) critical point is that $H_0^1(\Omega)$ is compactly embedded in $L^{p+1}(\Omega)$ (so that a sequence u_n bounded in H_0^1 is both bounded and has a convergent subsequence in L^{p+1}). For the *subcritical* case $p < 5$, this condition holds and the variational approach predicts that solutions of (1.1) exist for all $\lambda < \lambda_1$. The theory for this case, is reviewed in Lions [18]. For the *critical* case $p = 5$, $H_0^1(\Omega)$ is embedded in $L^{p+1}(\Omega)$ but this embedding is not compact and the existence of solutions cannot be guaranteed. Some extensions to the existence theory in this case are given by [5] and by [21]. For the *super critical* case $p > 5$, $H_0^1(\Omega)$ is not even embedded in $L^{p+1}(\Omega)$ and the variational approach breaks down completely. There are very few analytical results for this case and those that exist [5], [23] show that the questions of existence and uniqueness can be very delicate – with the possibility of multiple solutions or of singular weak solutions.

In this paper we restrict our attention to the most delicate critical case (1.1).

2.2 The Solution Branch

It is a straightforward application of bifurcation theory to show that if $p > 1$ a solution branch (λ, u) of (2.1) bifurcates from the trival solution $u = 0$ at $\lambda = \lambda_1(\Omega)$. This branch is unbounded in the joint norm of $|\lambda| + \|u\|_\infty$, exists in a left neighbourhood of λ_1 and is restricted to lie in the region $\lambda < \lambda_1$. Following the important result in [16] we may also deduce that the function u inherits the symmetries of Ω.

However, a significant non-existence result, showing that the breakdown of the variational approach is sharp, is due to Pohozaev [23] who showed that for any star-shaped domain

Ω, there is no solution of (2.1) if $\lambda = 0$ and $p \geqslant 5$. For $p = 5$ this result was extended in [5] to show that for any star-shaped domain there exists a critical value $\lambda_0 = \lambda_0(\Omega) > 0$ such that λ_0 is the infimum of the set of values of λ for which (1.1) has a solution. It is also known that solutions of (1.1) can exist when $\lambda = 0$ for domains which possess non-trivial topology [2] or which are not star-shaped [14]. The nature of the dependence of the existence of solutions to (1.1) on the domain Ω is thus an open and interesting question. Brezis and Nirenberg [5] give various upper bounds for λ_0, in particular they show that a solution exists if

$$\lambda \geqslant \lambda_* \equiv \frac{\pi^2}{4R^2} \tag{2.4}$$

where R is the radius of the largest ball that can be placed inside Ω. For example, if Ω is a cuboid domain of sides X, Y, Z then

$$\lambda_1 = \pi^2 \left(\frac{1}{X^2} + \frac{1}{Y^2} + \frac{1}{Z^2} \right). \tag{2.5}$$

and $\lambda_* = \pi^2/D^2$ where $D = \min\{X, Y, Z\}$. We show in Section 4 that λ_* is a poor estimate of λ_0 for such a domain.

Much more can be said when Ω is a sphere (wlog of radius 1) centred on the origin, as then the solutions of (1.1) are radially symmetric and satisfy an ordinary differential equation in $r = |\mathbf{x}|$. In particular it has been shown [5], [1] that u is unique and exists if and only if $\lambda \in (\lambda_0, \lambda_1)$ where $\lambda_1 = \pi^2$ and $\lambda_0 = \lambda_* = \frac{1}{4}\lambda_1$. As $\lambda \to \lambda_0$, $u(\mathbf{0}) = \|u\|_\infty \to \infty$ and $u(\mathbf{x}) \to 0$ if $\mathbf{x} \neq \mathbf{0}$. Furthermore, it is shown in [7],[6] that in this limit the following estimates apply

$$(\lambda - \lambda_0)\|u\|_\infty^2 \to \frac{\sqrt{3}\pi^3}{2}, \quad \|u\|_{H_0^1}^2 \to \frac{3^{3/2}\pi^2}{4}, \quad (\lambda - \lambda_0)^{-1}\|u\|_2^2 \to \frac{32\sqrt{3}}{\pi}. \tag{2.6}$$

2.3 The Nature of the Singularity

Arguing by analogy to the sphere it is conjectured that if Ω is a star-shaped domain, then $u(\mathbf{x})$ is a unique function of λ for $\lambda \in (\lambda_0, \lambda_1)$, which becomes infinite at a single point $\mathbf{x_0}$ as λ tends to λ_0 and which tends to zero at all other points. It is not known if this conjecture is true even for simple domains such as the cube or cuboid. The solution profiles presented in Figure 1.2 lend some support to this conjecture as they show a narrowing peak developing at the centre of the cube as λ is reduced, although (due to the errors in the numerical computation) there is no point λ_0 at which the illustrated solution becomes unbounded. As u is large at $\mathbf{x}_0$ the u^5 term in (1.1) dominates λu at this point. Elsewhere, where u is small, λu dominates u^5. Using this result we can crudely approximate the function u^5 in (1.1) by a scalar multiple $A\delta(\mathbf{x} - \mathbf{x_0})$ of the delta function leading to the approximation

$$\Delta u + \lambda u = -A\delta(\mathbf{x} - \mathbf{x}_0). \tag{2.7}$$

This equation has solution

$$u(\mathbf{x}) \approx AG_\lambda(\mathbf{x}, \mathbf{x_0}) \tag{2.8}$$

where G_λ is the Green's function for the Helmholtz operator $-\Delta u - \lambda u$. In Section 5 we derive an approximate value for A and compare (2.8) with the calculated solution. By studying this equation, McLeod [20] (see also [25], [4]) proved an upper estimate λ_{**} for λ_0. For the sphere it is known that $\lambda_{**} = \lambda_0$, and McLeod conjectured that this result will also hold for more general domains. For the cube, the value of λ_{**} can be computed accurately fairly easily, and we detail this calculation and give a precise definition for λ_{**} in Section 4. We then show that, up to the accuracy that we can compute λ_0 for the cube, the values of λ_0 and λ_{**} are equal.

The approximation of u^5 by a delta function is crude and the description of the solution when u is large can be improved by using some scaling arguments. To do this we presume (without loss of generality) that the maximum value of $u(\mathbf{x})$ occurs at the origin and define

$$\gamma = \|u\|_\infty = u(\mathbf{0}).$$

Now, introduce the scaled function $v(\mathbf{y})$ and scaled coordinate $\mathbf{y}$ defined by

$$u(\mathbf{x}) = \gamma v(\gamma^2 \mathbf{x}) \quad \text{and} \quad \mathbf{y} = \gamma^2 \mathbf{x}. \tag{2.9}$$

Rescaling the equation (1.1) and expressing all derivatives in terms of $\mathbf{y}$ we have

$$\Delta v + v^5 + \lambda \gamma^{-4} v = 0, \quad \|v\|_\infty = 1 \tag{2.10}$$

where $v = 0$ on $\partial\Omega_\gamma$ with Ω_γ a rescaling of Ω. For large γ it is evident that v approximately satisfies the simpler equation $\Delta v + v^5 = 0$ which, in the absence of boundary conditions has the radially symmetric solution

$$w(\mathbf{y}) = (1 + |\mathbf{y}|^2/3)^{-1/2}. \tag{2.11}$$

If γ is large then the boundary of Ω_γ is distant from the origin and can be expected to have only a small effect on the solution of (2.10). We make the reasonable conjecture that close to the origin v is also close to being radially symmetric and hence that $v(\mathbf{y}) \approx w(\mathbf{y})$. Rescaling this gives

$$u(\mathbf{x}) \approx w_\gamma(\mathbf{x}) \equiv \frac{\gamma}{(1 + \frac{1}{3}\gamma^4 |\mathbf{x}|^2)^{1/2}}. \tag{2.12}$$

The expression (2.12) gives a leading order approximation to $u(\mathbf{x})$ close to the singularity which becomes progrssively less accurate as $\mathbf{x}$ approaches the boundary of Ω. (In [17] it is shown that if u satisfies the related equation

$$\Delta u + u^{5-\varepsilon} = 0, \quad \varepsilon > 0 \tag{2.13}$$

then in the rescaled coordinates $v(\mathbf{y}) \to w(\mathbf{y})$ in any set for which $|\mathbf{y}|$ is bounded as $\varepsilon \to 0$.) The computations presented in Section 5 demonstrate that (2.12) is very descriptive for even quite large values of $|\mathbf{x}|$ and we use it subsequently as the basis of an asymptotic calculation both of u and for its finite element approximation U_h.

3 Qualitative Properties of the Discrete Equations

We now describe the basic finite element method used to calculate a discrete solution branch (λ, U_h) approximating the true solution branch (λ, u) of (1.1). We then make some preliminary observations about the underlying behaviour of the discrete solution and the problems encountered as the true solution becomes more singular.

3.1 Formulation of the finite element equations

The finite element method seeks a zero of the functional Ψ defined in (2.2) but now considered as a map from a *finite-dimensional* subspace $S_h(\Omega)$ of $H_0^1(\Omega)$ to its dual space $S_h^{-1}(\Omega)$. This is equivalent to finding a function $U_h \in S_h$ such that

$$-a(U_h,\varphi)+\langle \lambda U_h+U_h^5,\varphi\rangle=0, \quad \forall \varphi \in S_h. \tag{3.1}$$

The function U_h is also a saddle point in S_h of the function $\Phi(u)$ defined in (2.3). The existence of such a non-zero function U_h can, as before, be determined by applying the Mountain Pass Theorem. As the space S_h is finite dimensional, the embedding of S_h into L^{p+1} is compact for all values of $p \geqslant 1$. As a consequence we can deduce the following result.

Theorem 3.1 *A positive solution branch $(\lambda, U_h) \in \mathbb{R} \times S_h$ of (3.1) exists for all $p \geqslant 1$ and for all $\lambda < \lambda_1$.*

Proof. The proof follows immediately on applying the methods in [12] to the finite dimensional space S_h. More details are given in [9]. □

Note Applications of the Mountain Pass theorem to give constructive numerical algorithms for many problems are given in the paper of Choi *et al* [11]. □

If $\lambda > \lambda_0$ then such solutions should converge to the true solution of the underlying problem as the computational mesh is refined. However, if $\lambda < \lambda_0$ then they cannot converge and are spurious.

Now take Ω to be a cube centred on the origin with $-1/2 \leqslant x,y,z \leqslant 1/2$. We divide Ω into a regular lattice of cubic elements of side h with $S_h \subset H_0^1(\Omega)$ the space spanned by the basis functions $\varphi_i(\mathbf{x})$ which have as support the eight elements centred on the i^{th} node, are trilinear on these elements (ie. linear in each coordinate direction), continuous across the element boundaries, take the value 1 at the i^{th} node and are zero at all other nodes. Thus we may represent $U_h(\mathbf{x})$ as

$$U_h(\mathbf{x})=\sum_{i=1}^{N} U_i\varphi_i(\mathbf{x})$$

and may rewrite (3.1) as

$$-\sum_{i=1}^{N} U_i a(\varphi_i,\varphi_j)+\langle \lambda U_h+U_h^5,\varphi_j\rangle=0 \quad \forall j=1,\ldots,N. \tag{3.2}$$

For this calculation, the simple polynomial nature of the nonlinearity means that all integrals can be evaluated exactly by using Gaussian quadrature on each element with four integration points in each coordinate direction. The finite element method thus reduces the problem (3.1) to solving N coupled (nonlinear) equations for the unknowns $\boldsymbol{U}=[U_1,\ldots,U_n]^T \in \mathbb{R}^n$ and we may rewrite (3.2) as

$$K\mathbf{U}=\lambda A\mathbf{U}+\mathbf{G}(\mathbf{U}) \tag{3.3}$$

where $K_{ij} = a(\varphi_i, \varphi_j)$, $A_{ij} = \langle \varphi_i, \varphi_j \rangle$ and $[\mathbf{G}(\mathbf{U})]_i = \langle U_h^5, \varphi_i \rangle$. By solving (3.3) we can thus find a *branch* (λ, U_h) of solutions of the discrete weak equation (3.1). The arguments presented in [22] show that the branch so computed satisfies

$$\|U_h\|_\infty < C h^{-1/2},$$

where C depends upon the domain, but not on λ, h or U_h.

As will be clear in Section 5, it is necessary to take $N \approx 10^6$ nodes, which leads to severe computational difficulties in solving the algebraic systems. Our technique for finding the solution is to exploit the natural homotopy parameter λ and solve (3.3) by numerical continuation in this parameter given a suitable starting point, and making small reductions in λ at each step. For each such step we solve (3.3) by using a pseudo-Newton method for which the Jacobian of the problem is approximated by a related matrix with reduced memory allocation. These pseudo-Jacobian matrices are symmetric but not positive definite. The resulting linear systems are then solved by using the conjugate gradient method *without* preconditioning. There are two reasons why preconditioning is not used. Firstly, standard preconditioners are ineffective because the pseudo-Jacobian matrices are not positive definite, and secondly the unconditioned method converges relatively quickly. For an unpreconditioned system if the indefiniteness causes difficulties with the convergence of the conjugate gradient method, then this is readily seen. Although conjugate gradients is robust only for positive definite systems, we found no convergence difficulties for our (mildly) indefinite problems. For example, on a mesh of $100^3 = 10^6$ elements making a step of $\Delta\lambda = 0.5$ between sucessive values of λ then on average only 1.32 iterations of the Newton method and 210 inner iterations of the CG method are needed to obtain a convergent solution at each step. Further details and an analysis of the effectiveness of this solution procedure are given in [10].

3.2 Starting the branch

An application of standard bifurcation theory to the discrete problem (3.3) implies that there is a bifurcation of a non-trivial solution branch from the zero solution at the value $\lambda = \lambda_{1,h}$ where $\lambda_{1,h}$ is the smallest generalised eigenvalue of the system linearised about $\mathbf{U} = \mathbf{0}$ satisfying

$$K\psi_{1,h} = \lambda A \psi_{1,h}$$

with a non-zero vector $\psi_{1,h}$. This equation is a discretisation of the Helmholtz equation

$$-\Delta\psi_1 = \lambda\psi_1, \qquad \psi = 0 \quad \text{if} \quad \mathbf{x} \in \partial\Omega$$

satisfied (for non-zero ψ) when $\lambda = \lambda_1(\Omega)$ and from standard results in approximation theory we have that $\lambda_1 < \lambda_{1,h} = \lambda_1 + \mathcal{O}(h^2)$. For λ close to $\lambda_{1,h}$ the vector $\mathbf{U}$ is then close to the space spanned by $\psi_{1,h}$ and by using the Lyapunov-Schmidt reduction, its magnitude can be found by solving a simple one-dimensional nonlinear equation. Such a procedure is described in generality in [12]. For the unit cube (or indeed for general cuboid domains) the implementation is made easier by the fact that the eigenvalues and eigenfunctions are known explicitly with λ_1 given by (2.5) and

$$\psi_1(\mathbf{x}) = \psi_1(x, y, z) = \cos(\pi x)\cos(\pi y)\cos(\pi z).$$

In practice, taking $\lambda = \lambda_1$ initially and setting $U_h = \hat{\psi}_1$ with $\hat{\psi}_1$ the interpolant of ψ_1 in S_h, proved sufficiently accurate an initial guess to allow rapid convergence onto the solution branch.

3.3 Convergence of the Numerical Method

The study of the convergence of the discretisations of general semi-linear equations is not new. An overall theory (based upon the implicit function theorem or on concepts of non-linear stability) has been developed for the numerical approximation of isolated solutions of problems of the form (1.1) for fairly general functions $f(u;\lambda)$. Good references to this work are given in the monograph by Crouzeix & Rappaz [13], and also in the papers by Lopez-Marcos & Sanz-Serna [19] and Dobrowolski & Rannacher [15]. Such results typically assume that a solution U_h has been constructed in a neighbourhood of the true solution u and look at the convergence of U_h to u as the mesh is refined. Typically such convergence is expressed in the form

$$\|U_h - u\| < B(u)h^\alpha \log(1/h)^\beta \tag{3.4}$$

where $\| \bullet \|$ is a suitable norm and the values of $B(u)$, α and β depend upon that norm. For piecewise linear finite elements, we have [15]

$$\|U_h - u\|_\infty < B_\infty(u)h^2 \log(1/h) \quad \text{and} \quad \|U_h - u\|_{H_0^1} < B_H(u)h \tag{3.5}$$

When using these estimates it is important to note that in three dimensions, functions which are bounded in H_0^1 can be unbounded in L_∞. In Lopez-Marcos & Sanz-Serna [19] it is also shown that there exist neighbourhoods of u (called *stability balls*) in which U_h both exists and is unique. In Murdoch & Budd [22] these results were applied directly to problems of the form (1.1) and it was shown that the radii of the stability balls were mesh dependent and that spurious solutions could exist outside them.

For the estimates of $\|U_h - u\|_\infty$ the constant $B_\infty(u)$ is proportional both to $\|\Delta u\|_\infty = \|\lambda u + u^5\|_\infty$ and to the infinity norm of the operator L_λ^{-1} defined in (1.4). As both are unbounded as $\lambda \to \lambda_0$ the above estimate is hard to apply, and descriptive only when h is very small. Consequently, the result (3.5) does not give a completely satisfactory account of the convergence of a numerical method for (1.1).

3.4 Spurious Solutions of the Numerical Method

A secondary difficulty arises when $\lambda < \lambda_0$, as then the discrete equations admit spurious solutions. Obviously, it is very important to be able to distinguish spurious solutions from convergent approximations to solutions of (1.1). Whilst spurious solutions introduced by temporal discretisations (of ordinary differential equations) are now fairly well understood [26], much less is known about spurious solutions introduced by spatial discretisation, and distinguishing the convergent from the spurious numerical solutions is a far from trivial task. For general problems these solutions either vanish or diverge to infinity in $L^\infty(\Omega)$ as the mesh is refined. As we have existence of solutions for all $\lambda < \lambda_1$ it is the latter which applies for solutions of (3.3), however the solutions remain bounded in other norms. In particular we observe spurious solutions of (1.1) which remain bounded in $H_0^1(\Omega)$ under mesh refinement and tend to zero in $L^2(\Omega)$. As mentioned in the introduction, the divergence in L_∞ as the mesh is refined can be very slow; typically for spurious solutions of (1.1) we will see that $\|U_h\|_\infty \sim h^{-1/4} \sim N^{1/12}$ where N is the number of computational nodes. With such a slow rate of divergence of spurious solutions it is not computationally feasible to use fine enough meshes to clearly distinguish between a slowly growing spurious solution and a convergent solution. This motivates the calculations in Section 6 where asymptotic methods are used to distinguish between the two types of solution.

3.5 Resolution of the singularity

The main difficulty posed to the numerical method is an adequate resolution of the singularity conjectured to form as $\lambda \to \lambda_0$. A preliminary error analysis can be made by considering the rescaling (2.9) which can also be applied to the finite element discretisation. In, particular, suppose that

$$\gamma = \|U_h\|_\infty, \quad \mathbf{y} = \gamma^2 \mathbf{x} \text{ and } U_h(\mathbf{x}) = \gamma V_H(\gamma^2 \mathbf{x}) \tag{3.6}$$

where

$$H = \gamma^2 h. \tag{3.7}$$

Under this rescaling the $V_H(\mathbf{y})$ belongs to the space of functions spanned by piecewise trilinear basis functions defined on cubes of side H. In the rescaled variables, we have conjectured that close to its peak the rescaled function $v(\mathbf{y})$ has the approximate form

$$v(\mathbf{y}) \approx 1/(1 + |\mathbf{y}|^2/3)^{1/2}.$$

For V_H to approximate this function it is clearly necessary that $H \ll 1$. Standard error estimates then imply that we can approximate $v(\mathbf{y})$ to an accuracy of $\mathcal{O}(H^2)$ by using piecewise linear elements and hence, on the original mesh, we can approximate the rescaled function $w_\gamma(\mathbf{x})$ to an accuracy of $\mathcal{O}(h^2\gamma^5)$. Thus, a necessary condition for an accurate numerical solution of (1.1) is that H is small. Now, observe that whereas h is known, the value of H can only be determined subsequent to the computation. Moreover, the condition of H being small is not sufficient as we have no a-priori guarantee that the value of γ itself is correct. Thus, although the numerical method may be able to resolve the profile of the singularity, it may get its maximum value wrong. This turns out to be a second principle source of error and we return to this in Sections 5 and 6.

4 Critical values of λ Derived from the Linear Green's Function

4.1 McLeod's Conjecture.

For our first investigations of the solutions of the nonlinear partial differential equation problem (1.1) we study the solutions of the related *linear* problem (2.7) approximating (1.1) when u is large. A numerical study of this problem is rather simpler than that for (1.1) and yet gives insight into the behaviour of the large solutions and affords the possibility of determining the range of existence of the solutions of (1.1) without solving the fully nonlinear problem.

For general $\mathbf{x}, \mathbf{y}$ the Green's function for the Helmholtz operator satisfies the equation

$$\left.\begin{array}{rcll} \Delta G_\lambda(\mathbf{x},\mathbf{y}) + \lambda G_\lambda(\mathbf{x},\mathbf{y}) & = & -\delta(\mathbf{x}-\mathbf{y}), & \mathbf{x} \in \Omega, \\ G_\lambda(\mathbf{x},\mathbf{y}) & = & 0 & \mathbf{x} \in \partial\Omega, \end{array}\right\} \tag{4.1}$$

(where all spacial derivatives are expressed in terms of $\mathbf{x}$). Since

$$\Delta\left(\frac{1}{4\pi|\mathbf{x}-\mathbf{y}|}\right) = -\delta(\mathbf{x}-\mathbf{y}) \tag{4.2}$$

we may write

$$G_\lambda(\mathbf{x},\mathbf{y}) = \frac{1}{4\pi|\mathbf{x}-\mathbf{y}|} + g_\lambda(\mathbf{x},\mathbf{y}) \tag{4.3}$$

where the continuous but non-smooth function $g_\lambda(\mathbf{x},\mathbf{y})$ is called the *regular part* of the Green's function. It follows from (4.1) and (4.3) that

$$\left.\begin{aligned} \Delta g_\lambda(\mathbf{x},\mathbf{y}) + \lambda g_\lambda(\mathbf{x},\mathbf{y}) &= -\frac{\lambda}{4\pi|\mathbf{x}-\mathbf{y}|}, \qquad && \mathbf{x}\in\Omega, \\ g_\lambda(\mathbf{x},\mathbf{y}) &= -\frac{1}{4\pi|\mathbf{x}-\mathbf{y}|} && \mathbf{x}\in\partial\Omega. \end{aligned}\right\} \tag{4.4}$$

Following [4] we define the function $\varphi_\lambda(\mathbf{x}) \equiv g_\lambda(\mathbf{x},\mathbf{x})$, which plays a significant role in the theories both of problem (1.1) and of the closely related problem (2.13) (see [17],[24],[29]). In particular, McLeod [20] and Schoen [25] showed independently that if $\varphi_\lambda(\mathbf{x}) > 0$ for some point $\mathbf{x}$ in Ω then (1.1) has a solution. In Brezis [4] it is shown that $\varphi_\lambda(\mathbf{x})$ increases with λ and hence there is a unique $\lambda = \lambda_{**}$ and an $\mathbf{x_0}\in\Omega$ such that

$$\max(\varphi_\lambda(\mathbf{x}) : \mathbf{x}\in\Omega) = \varphi_\lambda(\mathbf{x}_0) = 0 \quad \text{if} \quad \lambda = \lambda_{**}.$$

Hence we have the following result.

Lemma 4.1 *The problem (1.1) has a solution if* $\lambda > \lambda_{**}$. □

McLeod conjectured that $\lambda_{**} = \lambda_0$, with the singularity in $u(\mathbf{x})$ forming at the point $\mathbf{x} = \mathbf{x}_0$. Strong numerical evidence supporting this conjecture is presented in the rest of this paper.

For the unit sphere centred on the origin, $\mathbf{x_0} = \mathbf{0}$ and if $0 < \lambda < \lambda_1$ then $\varphi_\lambda(\mathbf{0}) = -\lambda^{1/2}\cot(\lambda^{1/2})/4\pi$ giving $\lambda_{**} = \lambda_0 = \pi^2/4$. For less symmetric domains, both $\mathbf{x}_0$ and λ_{**} are hard to determine. The only result so far is due to Wang [28] who showed that if $E_{s,B} = \{x\in\mathbb{R}^3 : -s < x_1 < s, (x_2,x_3)\in B\}$ where B is any bounded domain then as $s\to 0$

$$\frac{\lambda_{**}(E_{s,B})}{\lambda_1(E_{s,B})} \to \frac{4}{9}.$$

Wang also conjectured that for any domain

$$\frac{1}{4} \leqslant \frac{\lambda_{**}}{\lambda_1} \leqslant \frac{4}{9}. \tag{4.5}$$

It is clear from the discussion above that a numerical computation of the function $g_\lambda(\mathbf{x},\mathbf{y})$ and hence of $\varphi_\lambda(\mathbf{x})$ has the potential of giving much insight into the solutions of (1.1). This computation requires the solution of a linear problem, which can be determined with great accuracy at relatively little cost. However, to determine $\varphi_\lambda(\mathbf{x})$ at a *single* point $\mathbf{x}$ we must calculate $g_\lambda(\mathbf{x},\mathbf{y})$ over the *whole* of the domain Ω. This makes the determination of λ_{**} a formidable task for a domain in which $\mathbf{x}_0$ is not known a-priori. However, in cuboid domains, centred on the origin, symmetry arguments imply that $\mathbf{x_0} = \mathbf{0}$ and hence, we need only consider the function $\varphi_\lambda(\mathbf{0})$ which is a much simpler computational task.

The equation (4.4) has a singularity as $|\mathbf{x}-\mathbf{y}| \to \mathbf{0}$ making computation difficult. Consequently, we solve a related problem which removes this singularity. In contrast to (4.3) we write

$$G_\lambda(\mathbf{x},\mathbf{y}) = \theta_\lambda(\mathbf{x},\mathbf{y}) + h_\lambda(\mathbf{x},\mathbf{y}) \tag{4.6}$$

where

$$\theta_\lambda(\mathbf{x},\mathbf{y}) = \frac{\cos(\lambda^{1/2}|\mathbf{x}-\mathbf{y}|)}{4\pi|\mathbf{x}-\mathbf{y}|}. \tag{4.7}$$

A simple calculation shows that

$$\Delta\theta_\lambda(\mathbf{x},\mathbf{y}) + \lambda\theta_\lambda(\mathbf{x},\mathbf{y}) = -\delta(\mathbf{x}-\mathbf{y}), \tag{4.8}$$

and substituting (4.6) into (4.1) and using (4.8) we obtain

$$\left.\begin{aligned} \Delta h_\lambda(\mathbf{x},\mathbf{y}) + \lambda h_\lambda(\mathbf{x},\mathbf{y}) = 0, \qquad & \mathbf{x}\in\Omega, \\ h_\lambda(\mathbf{x},\mathbf{y}) = -\theta_\lambda(\mathbf{x},\mathbf{y}) \qquad & \mathbf{x}\in\partial\Omega. \end{aligned}\right\} \tag{4.9}$$

If $y \notin \partial\Omega$ then the function θ_λ is smooth on the boundary of $\partial\Omega$. Thus, if $\lambda < \lambda_1$, standard results from the theory of elliptic partial differential equations predict that the function h_λ exists and (unlike g_λ, is smooth in the interior of Ω. Finally, using (4.3) and (4.6) it follows that

$$\begin{aligned} g_\lambda(\mathbf{x},\mathbf{y}) &= \theta_\lambda(\mathbf{x},\mathbf{y}) - \frac{1}{4\pi|\mathbf{x}-\mathbf{y}|} + h_\lambda(\mathbf{x},\mathbf{y}) \\ &= \frac{1}{4\pi|\mathbf{x}-\mathbf{y}|}\Big(\cos(\lambda^{1/2}|\mathbf{x}-\mathbf{y}|) - 1\Big) + h_\lambda(\mathbf{x},\mathbf{y}) \end{aligned} \tag{4.10}$$

To compute λ_{**} for cuboid domains with $\mathbf{x_0} = \mathbf{0}$ we solve (4.9) for $h_\lambda(\mathbf{x},0)$ using the finite element method with the same mesh and basis functions as in Section 3. Letting $\mathbf{x}\to\mathbf{0}$ in (4.10) then gives

$$\varphi_\lambda(\mathbf{0}) = g_\lambda(\mathbf{0},\mathbf{0}) = h_\lambda(\mathbf{0},\mathbf{0}). \tag{4.11}$$

The value of λ_{**} is determined by using path following in λ and interval bisection to find the unique value of λ_{**} such that $\varphi_{\lambda_{**}}(\mathbf{0}) = 0$. We note that as the function h_λ is smooth, then standard error estimates of the form (3.5) from the theory of the finite element method may be applied to estimate the accuracy of the above computation. As the value of θ_λ on $\partial\Omega$ depends smoothly upon λ, as does the inverse of the linear operator in (4.10) the constants implied in these calculations (unlike those in the calculation of the nonlinear equation) are largely independent of λ, and consequently we predict a consistently accurate solution.

4.2 Results

The following table presents calculated values of λ_{**} for Ω is a cube of side 1, using the finite element method described in Section 3. Here, $\lambda_{**}(h)$ is the numerical approximation to λ_{**} obtained by using mesh of side h.

h	$\lambda_{**}(h)$	C	λ_{**}
1/10	7.421711		
1/20	7.483804	8.279	7.504502
1/30	7.495309	8.283	7.504513
1/40	7.499337	8.287	7.504516
1/50	7.501201	8.284	7.504515
1/60	7.502212	8.271	7.504510
1/70	7.502823	8.289	7.504514
1/80	7.503220	8.304	7.504518
1/90	7.503491	8.259	7.504511
1/100	7.503685	8.274	7.504512
1/110	7.503829	8.297	7.504515

Studying the values presented in this table, we have strong evidence that asymptotically

$$\lambda_{**}(h) = \lambda_{**}(h) + Ch^2 + \mathcal{O}(h^3), \tag{4.12}$$

consistent with the second order convergence of the finite element method when using trilinear basis functions. Using two successively finer meshes we estimate C and λ_{**} to give the numbers in the third and fourth columns of the table. These strongly imply that for a cube of side 1

$$\lambda_{**} \approx 7.5045. \tag{4.13}$$

For this case, equation (2.4) gives the estimate $\lambda_0 \leqslant \lambda_* = \pi^2 = 9.8696$ whilst we can deduce from Lemma 3.1 that more precisely $\lambda_0 \leqslant \lambda_{**} = 7.5045$. Thus for the cube, (2.4) is certainly not sharp. Also note that $\lambda_{**}/\lambda_1 = 7.5045/3\pi^2 = 0.25345$. This lies between the two limits given by the conjecture in (4.5).

4.3 Estimates for the function $g(\mathrm{x}, \mathrm{y})$

The function $g(\mathbf{x}, \mathbf{0})$ plays an important role in the asymptotic analysis of (1.1) and we present some results here that will be needed in Section 6. From (4.10) we see that when Ω is any symmetric domain such as the cube, the function $\theta_\lambda(\mathbf{x}, \mathbf{0})$ is symmetric on the boundary of Ω. Consequently, the function $h(\mathbf{x}, \mathbf{0})$ is symmetric about the centre of the cube and thus satisfies

$$\nabla h_\lambda(\mathbf{0}, \mathbf{0}) = \mathbf{0}.$$

If $r = |\mathbf{x}|$ we therefore have $h_\lambda(\mathbf{x}, \mathbf{0}) = h_\lambda(\mathbf{0}, \mathbf{0}) + \mathcal{O}(r^2) = g_\lambda(\mathbf{0}, \mathbf{0}) + \mathcal{O}(r^2)$. Thus

$$g_\lambda(\mathbf{x}, \mathbf{0}) = \frac{1}{4\pi r}(\cos(\lambda^{1/2} r) - 1) + g_\lambda(\mathbf{0}, \mathbf{0}) + \mathcal{O}(r^2) = g_\lambda(\mathbf{0}, \mathbf{0}) - \frac{\lambda}{8\pi} r + \mathcal{O}(r^2), \tag{4.14}$$

noting that $g_\lambda(\mathbf{0}, \mathbf{0}) = 0$ if $\lambda = \lambda_{**}$.

5 Finite Element Solutions of the Full Nonlinear Problem

We now return to the nonlinear problem (1.1) and present the results of some computations. An asymptotic analysis of these computations is given in Section 6.

5.1 Bifurcation Diagrams

By computing the bifurcation diagram for $(\lambda, \|U_h\|)$ in various norms we can investigate the solution (and in particular the formation of the singularity) for a range of values of λ. A preliminary guide to the accuracy of this calculation is given by the local analysis of Section 3 which showed that the developing peak can only be realistically resolved if H as defined in (3.6) is small. Consequently, we label the corresponding meshes as *coarse* and *fine* depending upon the resulting value of H. An immediate difficulty with this computation is that whereas the value of h is known a-priori, the value of γ (which is a strongly non-linear function of h) and a mesh can only be classified as coarse or fine subsequent to a numerical calculation. As discussed in Section 3, having a fine mesh does not guarantee the accuracy of the calculation. However, we show that the solutions on the fine meshes obey scaling laws making them amenable to asymptotic analysis.

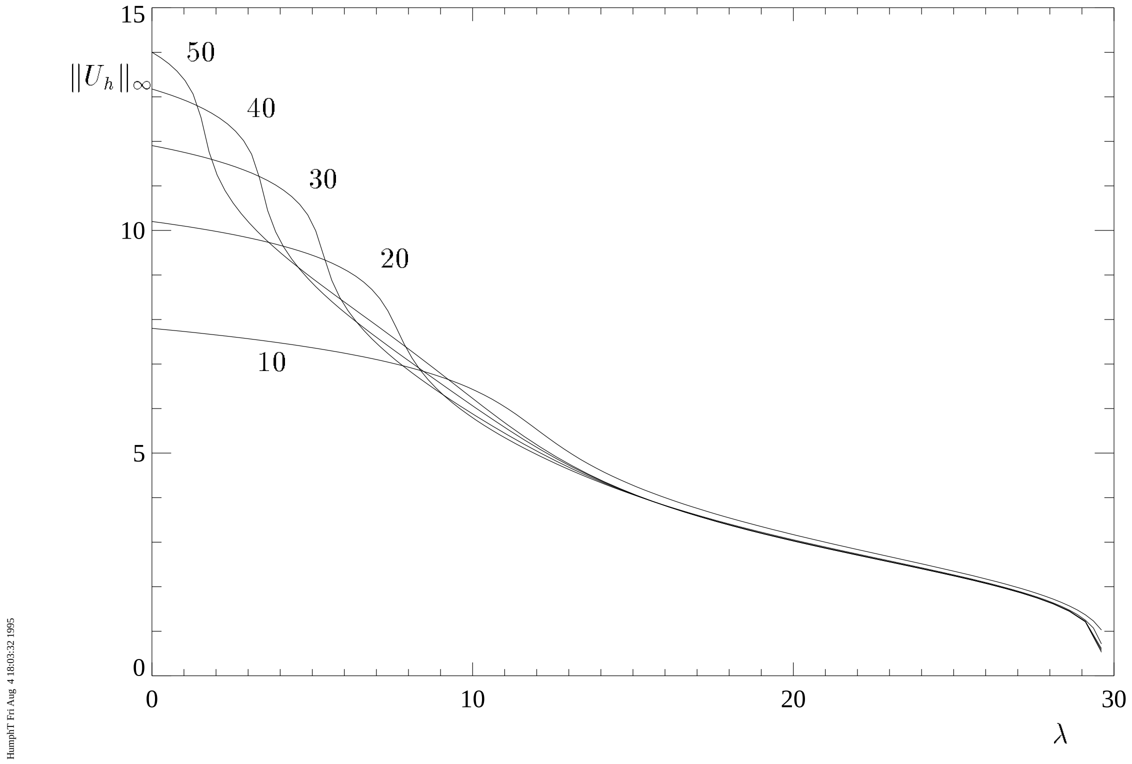

Figure 5.1: Bifurcation diagram of $\|U_h\|_\infty$ against λ, for coarse grids varying between $h = 1/10$ and $h = 1/50$.

5.1.1 Coarse mesh solutions

Our initial calculations for (1.1) were made with a mesh varying from $h = 1/10$ to $h = 1/50$. Whilst the case of $h = 1/10$ corresponds to 10^3 elements and can certainly be regarded as coarse, a mesh with $h = 1/50$ has 1.25×10^5 elements and may intuitively be regarded as fine. However, results on this mesh, although looking reasonable, are misleading as H is large. We present these results here to give some insight into the nature of truly spurious solutions which do not in any way resolve the singularity in u and from which little useful information can be extracted, leaving calculations on finer meshes to the next subsection.

In Figure 5.1 we plot the bifurcation diagram of $\|U_h\|_\infty$ as a function of λ for $h = 1/10, \ldots, 1/50$.

From this figure it is evident that a solution branch of the numerical discretisation does exist (as predicted) for all $\lambda < \lambda_1$. A steep gradient appears to form in each of these figures, and the value of λ at which this occurs decreases as the mesh is refined. This gives the misleading picture that λ_0 is close to zero. However, we observe that as the mesh is refined, there is little agreement between any of the curves when $\lambda \leqslant 13$ and the structures observed for this range of λ should be viewed with suspicion. A qualitative indication of this is the non-monotonicity of the graph of $\|U_h\|_\infty$ under mesh refinement, leading to a braiding structure in the bifurcation diagram.

A useful measure of the error of the solution is given by the value of H when $\lambda = \lambda_{**}$. In particular we have $H = 4.914$ if $h = 1/10$ and $H = 1.157$ if $h = 1/50$.

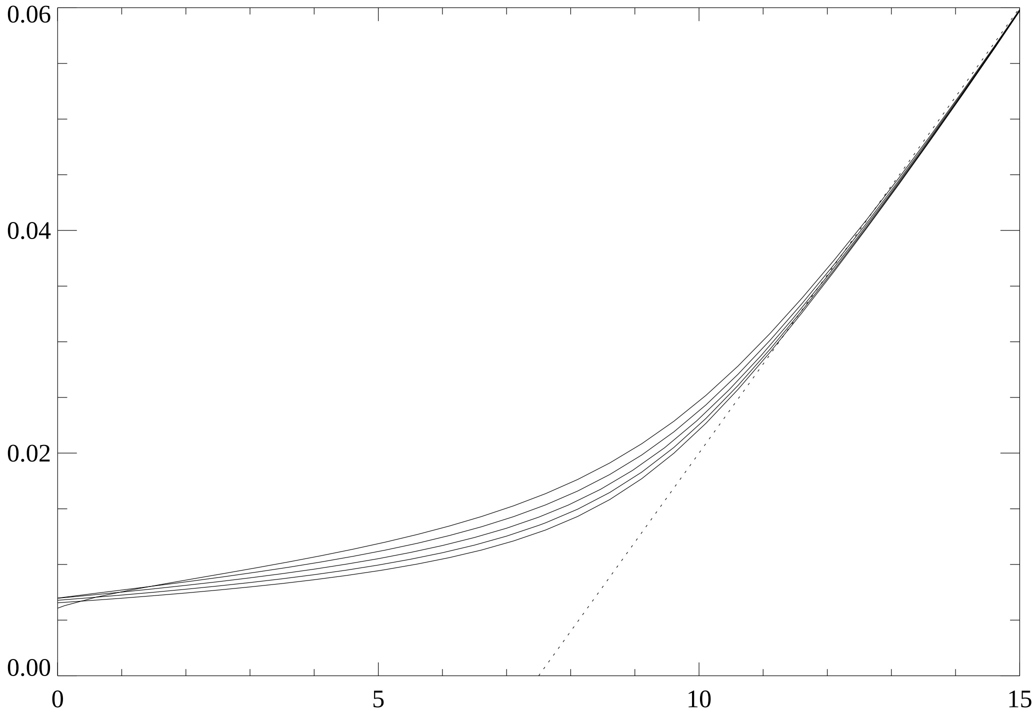

Figure 5.2: Bifurcation diagram of $1/\|U_h\|_\infty^2$ against λ, for grids varying between $h = 1/60$ and $h = 1/100$. For moderate values of λ ($\lambda \in [5, 10]$) the value of $1/\|U_h\|_\infty^2$ decreases monotonically as the mesh is refined.

5.2 Bifurcation Diagrams for the Fine mesh solutions in various norms

We now look at computations on finer meshes for which H takes smaller values than previously and for which the results obey a detectable asymptotic scaling law as $h \to 0$.

5.2.1 The Maximum Norm

A plot of $\|U_h\|_\infty$ against λ for values of the mesh size from $h = /60$ to $h = 1/100$ (10^6 elements) was presented in Figure 1.1. The solution branches for all these meshes agree for $\lambda \gtrapprox 12$ and for smaller values of λ this figure is strikingly different to Figure 5.1 Excepting the case of the $h = 1/60$ branch near $\lambda = 0$, we see that the value of $\|U_h\|_\infty$ is monotonically increasing as the mesh is refined; avoiding the braiding seen earlier. In this case the value of H when $\lambda = \lambda_{**}$ decreases from $H = 1.032$ when $h = 1/60$ to $H = 0.774$ when $h = 1/100$. Although this value is still not very small, it appears to be small enough for the asymptotic theory we will develop to be descriptive. It is revealing to also plot $1/\|U_h\|_\infty^2$. This is given in Figure 5.2. For the sphere we see from (2.6) that $1/\|u\|_\infty^2$ is proportional to $\lambda - \lambda_0$ if λ is close to λ_0. In Figure 5.2 we see that the corresponding curve for $1/\|U_h\|_\infty^2$ in the cube is approximately linear for $12 < \lambda < 15$ but departs from linearity as λ is reduced. Extrapolating the linear section gives an intercept (indicated) at a value of λ close to λ_{**}. In Section 7 we will demonstrate much stronger reasons for believing that $\lambda_0 = \lambda_{**}$.

Below we present a table of $||U_h||_\infty$ for various values of λ between 0 and 10, with mesh sizes between $h = 1/10$ and $h = 1/100$. For any fixed value of λ in the table the value of $||U_h||_\infty$ is ultimately monotonically increasing as the mesh is refined, however the smaller the value of λ the finer the mesh must be taken before this monotonicity is observed and any scaling law becomes apparent.

Mesh	λ										
Size	0	1	2	3	4	5	6	7	8	9	10
1/10	*7.80*	*7.73*	*7.65*	*7.57*	*7.47*	*7.37*	*7.24*	*7.10*	*6.92*	*6.71*	*6.43*
1/20	*10.20*	*10.10*	*9.98*	*9.84*	*9.67*	*9.44*	*9.13*	*8.56*	*7.27*	*6.36*	5.79
1/30	*11.91*	*11.75*	*11.57*	*11.32*	*10.95*	*10.17*	*8.32*	7.47	6.86	6.35	5.88
1/40	*13.18*	*12.93*	*12.57*	*11.86*	*9.76*	8.82	8.16	7.60	7.08	6.57	6.06
1/50	*14.00*	*13.40*	*11.30*	10.20	9.50	8.92	8.39	7.87	7.34	6.79	6.23
1/60	*12.84*	*11.51*	10.79	10.21	9.68	9.18	8.68	8.15	7.59	6.99	6.37
1/70	11.97	11.39	10.89	10.41	9.94	9.47	8.97	8.43	7.83	7.18	6.48
1/80	11.98	11.53	11.10	10.66	10.22	9.75	9.24	8.69	8.05	7.34	6.58
1/90	12.14	11.74	11.34	10.92	10.49	10.03	9.51	8.93	8.25	7.48	6.66
1/100	12.35	11.98	11.60	11.19	10.76	10.29	9.77	9.16	8.44	7.61	6.73

This table clearly indicates the difficulties in determining the difference between a convergent and a spurious solution. For $\lambda > \lambda_{**} = 7.5045$, Lemma 4.1 gives the existence of a solution of (1.1) and consequently U_h will converge toward this solution as $h \to 0$. However, it is almost impossible from an a-priori inspection to differentiate between a convergent solution at $\lambda = 8$ and a potentially spurious solution at $\lambda = 7$. To demonstrate this we plot in Figure 5.3 the value of $||U_h||_\infty$ for $\lambda = 6, 7, 8, 9, 10$ as h is refined, noting that the latter three graphs all correspond to convergent solutions. For sufficiently small h each of these graphs takes on a regular appearance which appears to indicate a regular and slow growth in $||U_h||_\infty$ as h is reduced, although we note that this is not inconsistent with convergence, only that h is not sufficiently small for convergence to be apparent for the meshes used.

Now taking $\lambda = \lambda_{**}$ we study this asymptotic growth in more detail. In the following table we present $||U_h||_\infty$ and $h^{1/4}||U_h||_\infty$, for varying h and also estimates of C and p obtained by applying the formula $\gamma = Kh^p$ to successive entries in the table through $p = (\log(||U_{h_1}||_\infty) - \log(||U_{h_2}||_\infty))/((\log h_1 - \log h_2)))$ and $K = (||U_{h_2}||_\infty)(h_2^p)$. These results imply strongly that p is close to 1/4 and are fully consistent with the predictions of the formal asymptotic formula (1.7) which we establish in Section 7.

h	$\|\|U_h\|\|_\infty$	$h^{1/4}\|\|U_h\|\|_\infty$	p	K
1/10	7.018735	3.947		
1/20	7.992000	3.779	-0.1873	4.559
1/30	7.146795	3.054	0.2757	18.252
1/40	7.334479	2.916	-0.0901	5.260
1/50	7.604458	2.860	-0.1620	4.035
1/60	7.875852	2.830	-0.1923	3.583
1/70	8.133509	2.812	-0.2088	3.349
1/80	8.374874	2.800	-0.2190	3.208
1/90	8.600438	2.792	-0.2256	3.116
1/100	8.811953	2.787	-0.2306	3.047

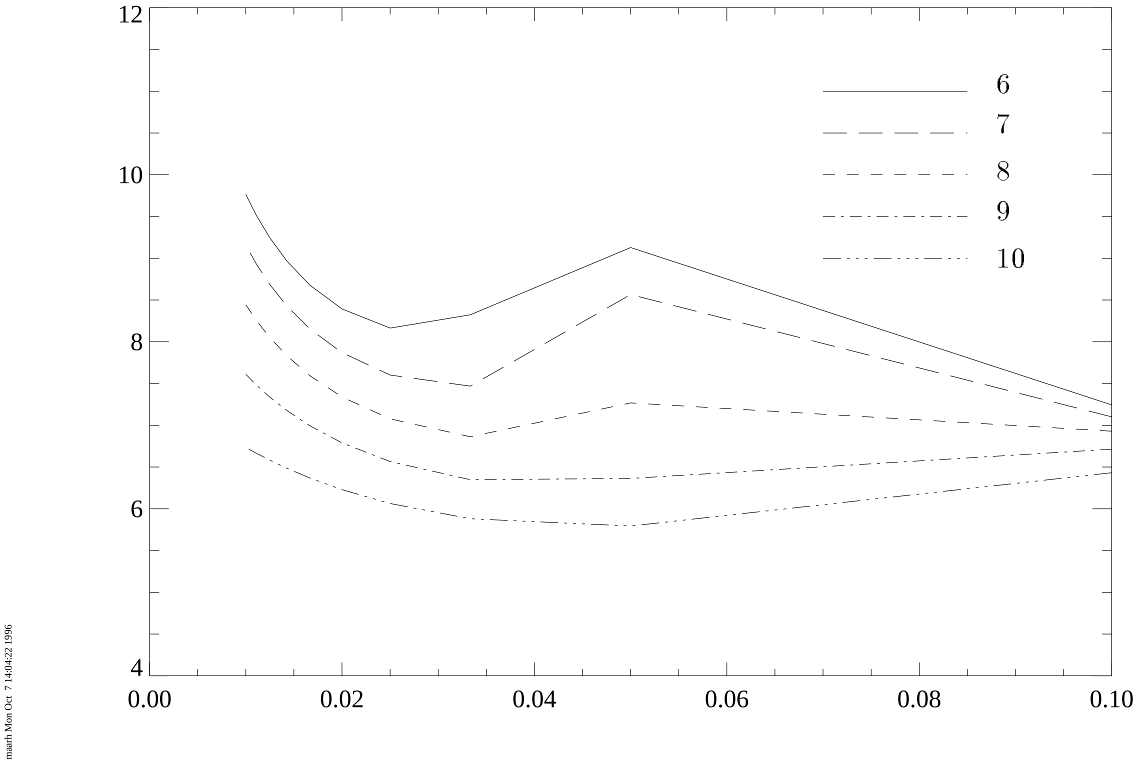

Figure 5.3: The value of $\|U_h\|_\infty$ as a function of h in the cases of $\lambda = 6, 7, 8, 9, 10$.

More generally the results in Section 7 imply that if λ is close to but larger than λ_0 then for h lying in the range $\|u\|_\infty^{-4} \ll h \ll \|u\|_\infty^{-2}$ the value of $\|U_h\|_\infty$ grows as $h^{-1/4}$ before converging to $\|u\|_\infty$ for smaller values of h.

5.2.2 The Sobolev norm

In Figure 5.4 we display the solution branches in the $H_0^1(\Omega)$ norm. We note from this figure that the values of $\|U_h\|_{H_0^1}$ appear to converge (to a value between 3.5 and 4) as $h \to 0$. Also away from the bifurcation point $\|U_h\|_{H_0^1}$ is roughly constant as λ is varied, although its maximum norm γ is changing. Observe that if $w_\gamma(\mathbf{x})$ is defined as in (2.12) then

$$\|w_\gamma\|_{H^1(\mathbf{R}^3)} = 3^{3/4}\pi/2 = 3.58063 \tag{5.1}$$

which is both independent of γ and close to the converged value. As the greatest contribution to the Sobolev norm of both u and of w_γ comes from the contribution due to the peak, this result is consistent with the conjecture made in Section 2 that in the peak u is closely approximated by w_γ.

5.3 The form of the solution.

From the calculations on the fine meshes we may draw some preliminary conclusions as to the form of the solution, in particular evidence for uniqueness, singularity and symmetry. We summarise these here.

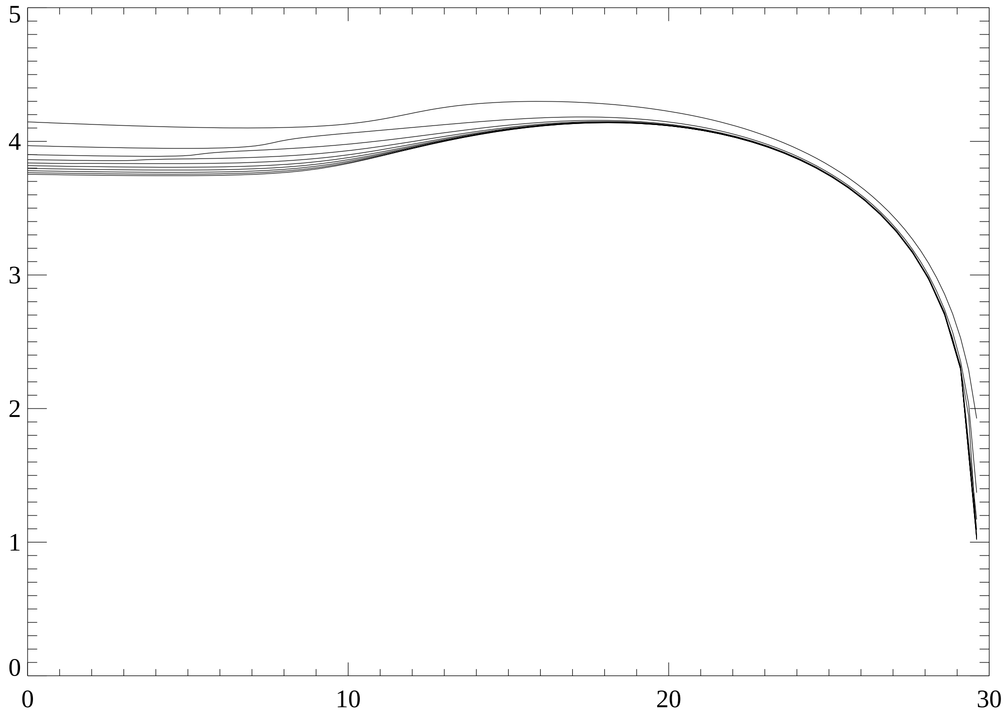

Figure 5.4: Bifurcation diagram of $\|U_h\|_{H_0^1}$ against λ, for grids varying between $h = 1/10$ and $h = 1/100$. The value of $\|U_h\|_{H_0^1}$ is monotonically decreasing as the mesh is refined.

5.3.1 Uniqueness

An initial, simple but important observation for the cube is that the solution branch bifurcates monotonically to the left, so that $\|U_h\|_\infty$ increases as λ decreases. In particular, there are no fold bifurcations or transcritical bifurcations on the branch and the solutions on the main branch appear to be unique for all values of $\lambda < \lambda_1$. All attempts to find additional solutions by starting from a point far distant from the main branch failed to give anything new. Accordingly we make the conjecture that the solutions of (1.1) are *unique* in cuboid domains.

5.3.2 The behaviour close to the peak

In Section 2 we discussed two descriptions of the approximation, namely approximating u^5 by a delta function and approximating u by the function w_γ. Some support for these has already been given by the results presented in Figure 1.2. To make this comparison more precise, we take $\lambda = \lambda_{**}, h = 1/100$ for which we find that $\gamma \equiv \|U\|_\infty = 8.812$. In Figure 5.5 we compare U_h with w_γ. In both cases a section of the function is taken along the line $x = y = z$ with $r = \sqrt{x^2 + y^2 + z^2}$. For comparison on this graph we also plot the function $f(\mathbf{x}) \equiv 4\pi\sqrt{3}G_\lambda(\mathbf{x}, \mathbf{0})/\gamma$. (The choice of the multiplicative constant will be made clear in Section 5.3.3).

This figure is very significant; it leads naturally to the asymptotic analysis that follows in Section 6. Note that the approximation of U_h by w_γ is very good if $r < 0.2$, for

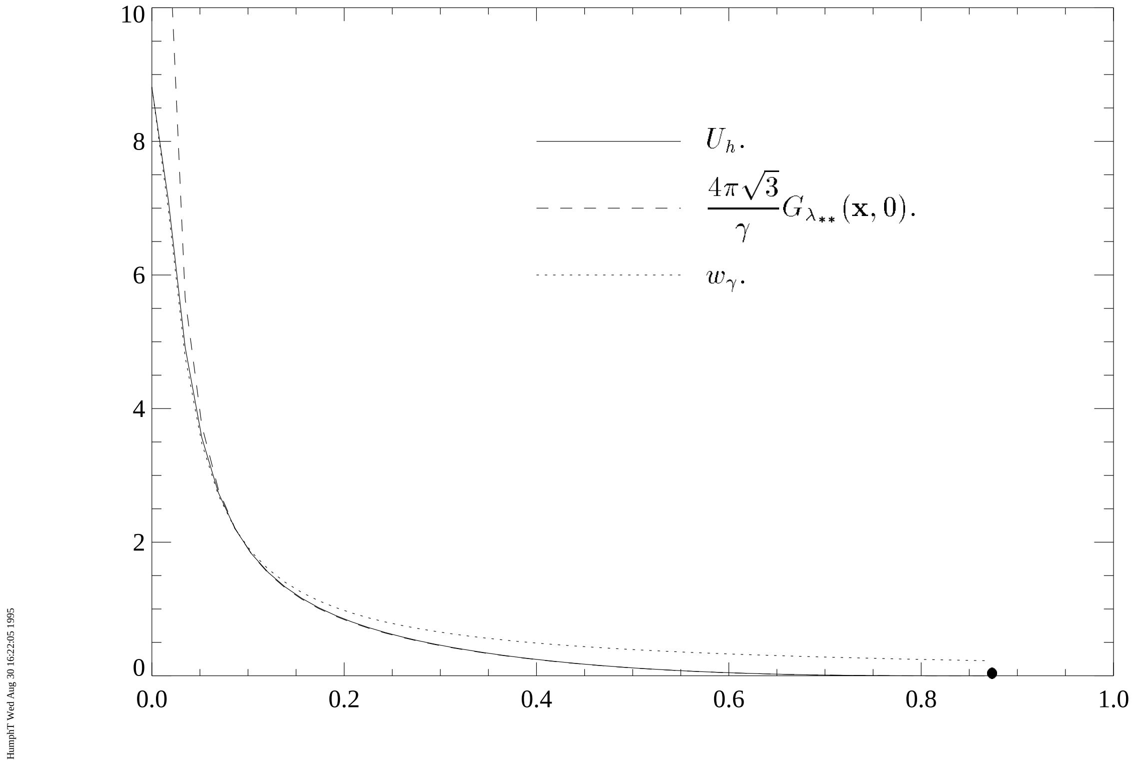

Figure 5.5: Graph of $U_h(\mathbf{x})$ and $w_\gamma(r)$ against $r = |\mathbf{x}|$ along the long diagonal $x = y = z$ of the cube, with $h = 1/100$, $\lambda = \lambda_{**} = 7.5045$ and $\gamma = \|U_h\|_\infty$. Also plotted is a scaling of the Green's function (4.3) of the linearized problem. Note that the point $r = \sqrt{3/4} = 0.866$ corresponds to a corner of the cube.

example $|U_h - w_\gamma|/w_\gamma < 0.15$ throughout this range, and near coincidence of the graphs as r reduces. Conversely the approximation of U_h by f is very good if $r > 0.05$ with again near coincidence of the graphs. Significantly these two ranges overlap.

In Figure 5.6 we give a section of the solution U_h with associated contours, through the plane $z = 0$. This figure gives a strong indication that U_h is close to being radially symmetric for even moderately large values of $\mathbf{x}$.

To make a quantitative assessment of this symmetry and also to compare $U_h(\mathbf{x})$ with the (radially symmetric function) $w_\gamma(\mathbf{x})$ more carefully we calculate the function $e(\mathbf{x}) \equiv U_h(\mathbf{x}) - w_\gamma(\mathbf{x})$ over the same range of parameters as before, considering the three lines $l_1 \equiv \{(x,y,z) : y = z = 0\}$, $l_2 \equiv \{(x,y,z) : x = y, z = 0\}$ and $l_3 \equiv \{(x,y,z) : x = y = z\}$. The resulting three curves are then plotted in Figure 5.7 This latter graph makes it clear both that U_h is close to w_γ over a wide range and also that the function $e(\mathbf{x})$ is itself very close to being radially symmetric. Indeed if $|\mathbf{x}| < 0.3$, then the estimates for $e(\mathbf{x})$ on the three radii differ by at most $|e(\mathbf{x})|/8$ with often better agreement. We make use of both of these observations in our asymptotic computations.

5.3.3 Behaviour away from the peak

It is clear from Figure 5.5 that away from the peak that U_h is close to $4\pi\sqrt{3}G_\lambda/\gamma$. This is consistent with the approximation for u given in (2.7) for which we had $u = AG_\lambda(\mathbf{x},\mathbf{0})$.

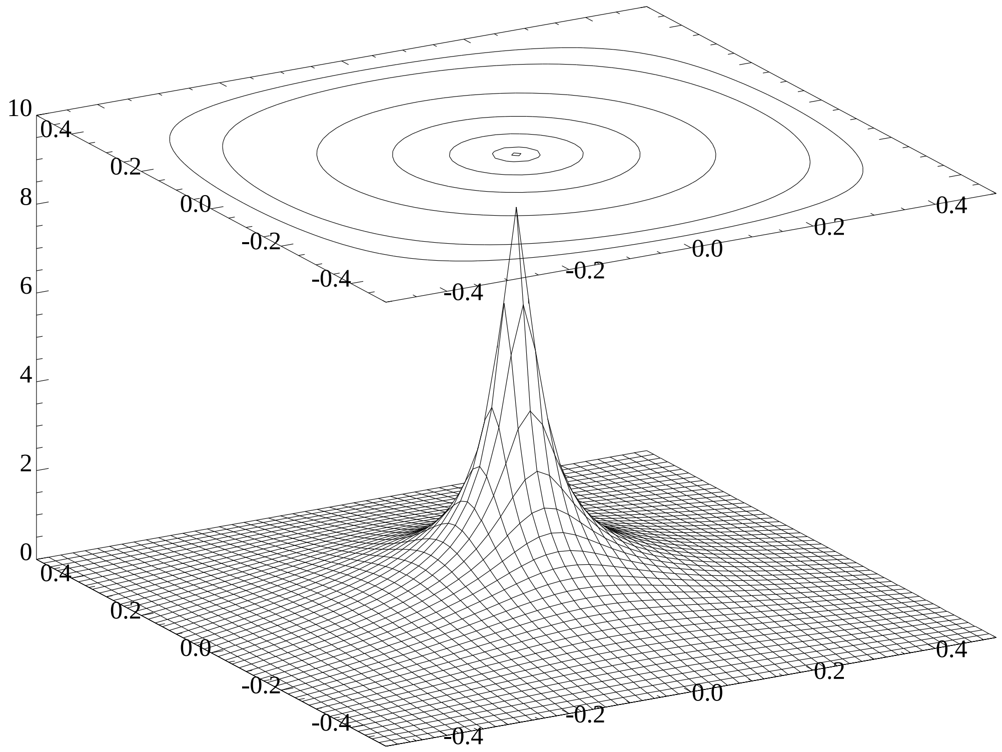

Figure 5.6: A cross section of U_h through centre of cube with $h = 1/100$ and $\lambda = \lambda_{**} = 7.5045$, with a contour plot which clearly shows the radial symmetry of the solution in the centre of the domain.

From Section 4 we have that

$$G_\lambda(\mathbf{x}, \mathbf{0}) = \frac{1}{4\pi|\mathbf{x}|} + g_\lambda(\mathbf{x}, \mathbf{0}). \tag{5.2}$$

Now, if γ is large, $\gamma^2|\mathbf{x}|$ is large and $|\mathbf{x}|$ is small then

$$w_\gamma(\mathbf{x}) \approx \frac{\sqrt{3}}{\gamma|\mathbf{x}|} \quad \text{and} \quad AG_\lambda(\mathbf{x}, \mathbf{0}) \approx A/4\pi|\mathbf{x}|,$$

so the two approximate descriptions of u agree to leading order if

$$A \approx A_1 \equiv 4\pi\sqrt{3}/\gamma.$$

leading to the choice made in Figure 5.5. By making a small change to this result and taking $A = 1.012 \times 4\pi\sqrt{3}/\gamma$ then the agreement is even better, with the functions nearly coinciding. The reason for this small correction will be made evident in the next section. A comparison is made in Figure 5.8 of the difference between these two functions in this case along the three radii taken before.

From this discussion we infer the following description of U_h if γ is large.

- There is an (inner) region $|x| < r_1$ such that U_h is close to the radially symmetric function w_γ. Furthermore the departure of U_h from radial symmetry is much smaller than the difference $|U_h - w_\gamma|$.

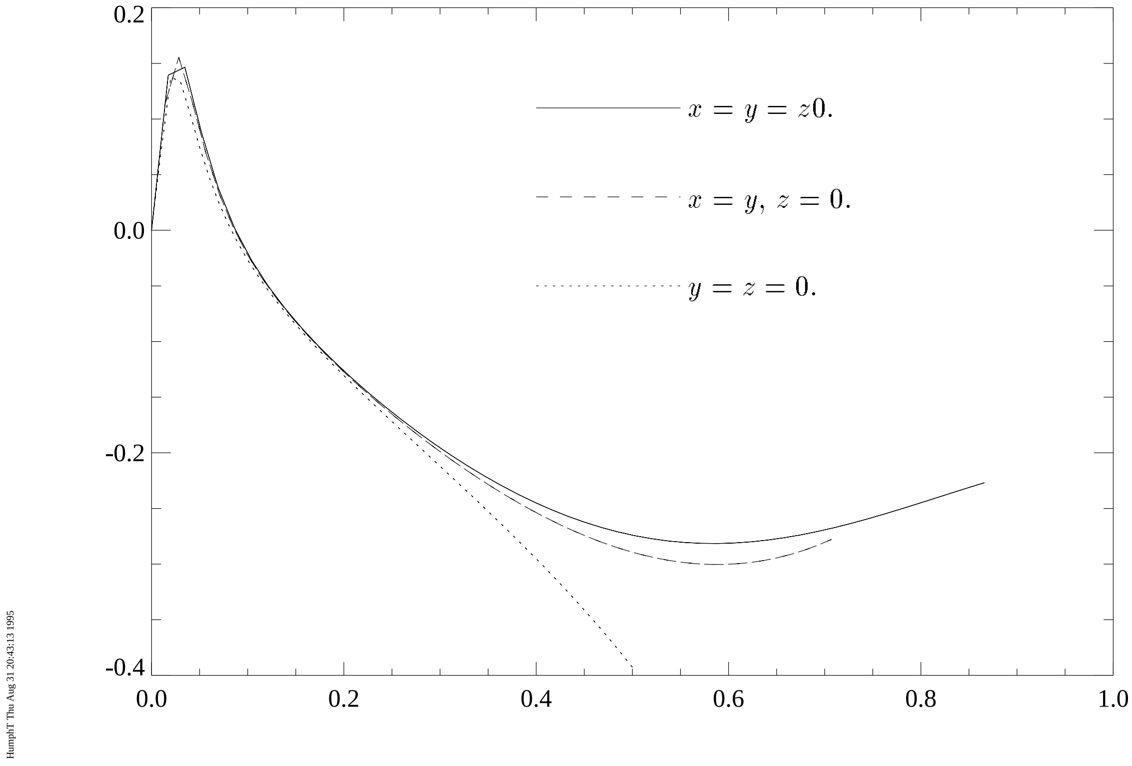

Figure 5.7: Graphs of $U_h(\mathbf{x}) - w_\gamma(\mathbf{x})$ against $|\mathbf{x}|$ along the three radii indicated, for $h = 1/100$ and $\lambda = \lambda_{**} = 7.5045$.

- There is an (outer) region $|x| > r_2$ such that u is close to AG_λ for appropriate A.

Significantly, our numerical calculations strongly indicate that r_2 is somewhat less than r_1 and that both approximations are good in the annulus $r_2 < |\mathbf{x}| < r_1$. Note further, that for $\lambda = \lambda_{**}, h = 1/100, \gamma = 8.812$ we can take $r_2 = 0.05, r_1 = 0.2$. In the rescaled variable $\mathbf{y} = \gamma^2 \mathbf{x}$ we have $\gamma^2 r_2 = 3.87$ and $\gamma^2 r_1 = 15.49$, so that, whilst r_1 is small, in the rescaled variables the corresponding value is relatively large. This is important for the analysis in the next section.

6 Asymptotics

Motivated by the above calculations we now develop a descriptive asymptotic theory. The results of the numerical calculations reported in the previous section have allowed us to draw some preliminary conclusions about the form of the solutions of (1.1) but are imprecise due to the relative coarseness of the discretisation. To continue our discussion we now make a formal asymptotic calculation of the nature of the continuous solution $u(\mathbf{x})$ based upon the numerical observations. We then extend this calculation in a natural way to look at the additional effects of the numerical discretisation. This calculation then allows us to post-process the numerical results to obtain a more accurate picture of the form of the solution. This calculation extends those given in [22] and [9].

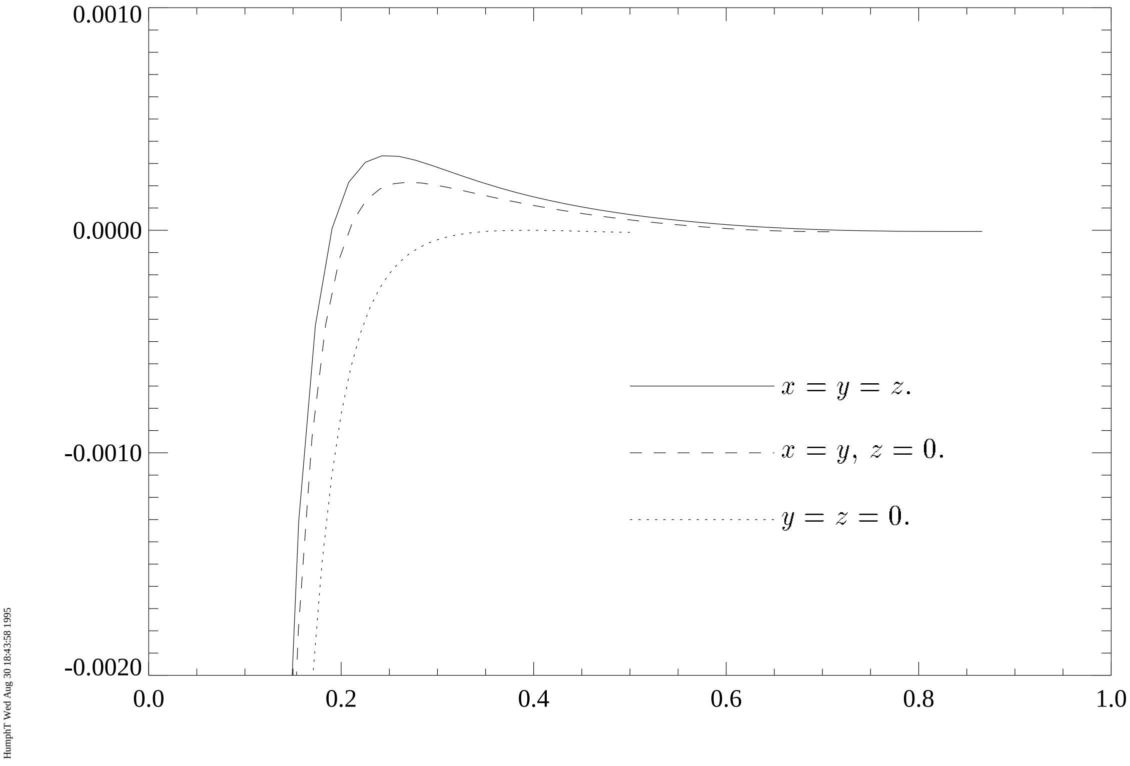

Figure 5.8: Graphs of $U_h(\mathbf{x}) - 1.012\frac{4\pi\sqrt{3}}{\gamma}G_{\lambda_{**}}$ against $|\mathbf{x}|$ along the same three radii indicated, with $\gamma = \|U_h\|_\infty$, $h = 1/100$ and $\lambda = \lambda_{**} = 7.5045$.

6.1 Formal asymptotic description of the continuous solution $\boldsymbol{u}$ when γ is large

For this calculation we look at the function $u(\mathbf{x})$ which we assume has a large peak centred on the origin. We then divide Ω into an *inner* region which includes the origin and for which $|\mathbf{x}|$ is small and an *outer* region which excludes the origin but includes the boundary of Ω. These regions are assumed to intersect in the annulus $r_2 < |\mathbf{x}| < r_1$. In the inner region we extend the analysis of Section 2 by rescaling $\mathbf{x}$ and u to $\mathbf{y}$ and v respectively and express v as a perturbation of w_1. This perturbation takes on a simple asymptotic form when $|\mathbf{y}|$ is large. In the outer region we extend the analysis of the previous section to express u as a perturbation of AG_λ, this also takes a simple asymptotic form when $|\mathbf{x}|$ is small. These two expressions for u are then matched in the annulus where both are valid. The matching region is chosen so that we can simultaneously take $|\mathbf{x}|$ to be small and $|\mathbf{y}|$ to be large. Observe that this is consistent with the results of the numerical calculations.

6.1.1 The Inner Region

Under rescaling (1.1) becomes

$$\Delta v + v^5 = -\lambda v/\gamma^4 \quad v = 0 \text{ on } \Omega_\gamma \tag{6.1}$$

where Ω_γ is an appropriately rescaled domain and the Laplacian now expresses derivatives with respect to $\mathbf{y}$. Motivated by this formula we express the function $v(\mathbf{y})$ for large γ as an asymptotic expansion in the form

$$v(\mathbf{y}) = v_1(\mathbf{y}) + v_2(\mathbf{y})/\gamma^4 + v_3(\mathbf{y})/\gamma^8 + ... \tag{6.2}$$

where γ is defined such that $v(\mathbf{0}) = 1$. Substituting into (6.1) and considering the leading order terms gives $\Delta v_1 + v_1^5 = 0$ so that (as predicted)

$$v_1(\mathbf{y}) = w_1(\mathbf{y}) = 1/\sqrt{1 + |\mathbf{y}|^2/3}.$$

Now considering terms of $\mathcal{O}(\gamma^{-4})$ we have

$$\Delta v_2 + 5w_1^4 v_2 = -\lambda w_1. \tag{6.3}$$

The function v_2 is a rescaling of $e \equiv u - w_\gamma$ which we have shown numerically is both small in comparison to w_γ and close to radially symmetric for a range of $\mathbf{x}$ over which $|\mathbf{y}|$ is large. Motivated by this we calculate v_2 over a non-empty sub-domain $\mathcal{A}$ of Ω_γ for which $|\mathbf{y}|$ is large but for which the non-radial component of v_2 can be ignored to the level of approximation considered. For large $|\mathbf{y}|$ we have

$$w_1(\mathbf{y}) = \sqrt{3}/|\mathbf{y}| + \mathcal{O}(1/|\mathbf{y}|^3) \gg w_1^4 \sim 9/|\mathbf{y}|^4$$

so that for this range

$$\Delta v_2 = -\frac{\lambda\sqrt{3}}{s} + \mathcal{O}(1/s^3), \text{ where } s = |\mathbf{y}|. \tag{6.4}$$

This equation has the radially symmetric solution

$$v_2(s) = \frac{a}{s} + b - \frac{\lambda\sqrt{3}}{2}s \tag{6.5}$$

where a and b are undetermined at this stage. Compare this description with the graph of $e(\mathbf{x})$ in Figure 5.7. Good agreement is observed for the range $0.05 < |\mathbf{x}| < 0.2$. For larger values of $|\mathbf{x}|$ terms of order $|\mathbf{x}|^2$ become significant, however, as these are of order $|\mathbf{y}|^2/\gamma^2$ they do not appear at this level of asymptotics.

The contribution to v_2 by the term b is important for the matching procedure and can be estimated by quadrature. Differentiating the function $w_\gamma(\mathbf{x})$ with respect to γ and setting $\gamma = 1$ we have that the function

$$\psi(\mathbf{y}) = (1 - |\mathbf{y}|^2/3)/(1 + |\mathbf{y}|^2/3)^{3/2} \tag{6.6}$$

satisfies the partial differential equation

$$\Delta\psi + 5w_1^4\psi = 0. \tag{6.7}$$

Multiplying (6.3) by ψ, (6.7) by v_2, subtracting and integrating over an arbitrary domain $\Omega' \subset \Omega_\gamma$ gives

$$\int_{\Omega'} (v_2\Delta\psi - \psi\Delta v_2)\, dV = \lambda \int_{\Omega'} w_1\psi dV. \tag{6.8}$$

Applying the divergence theorem we have

$$\int_{\partial\Omega'} (v_2\nabla\psi - \psi\nabla v_2)\, .\mathbf{dS} = \lambda \int_{\Omega'} w_1\psi dV. \tag{6.9}$$

Now take Ω' to be a sphere of radius $S \gg 1$ centred on the origin for which $\partial\Omega' \subset \mathcal{A}$. Using the form (6.5) for v_2 and (6.6) for ψ we have (after some manipulation) that

$$\int_{\partial\Omega'} (v_2 \nabla \psi - \psi \nabla v_2) \,.\mathbf{dS} = 4\pi \left[\sqrt{3} b - 3S\lambda + O\left(\frac{1}{S}\right) \right]. \tag{6.10}$$

Similarly, we have (by direct integration)

$$\lambda \int_{\Omega'} w_1 \psi dV = 4\pi \left[-3S\lambda + 3\sqrt{3}\pi\lambda + \mathcal{O}\left(\frac{1}{S}\right) \right] \tag{6.11}$$

Comparing the expressions (6.9), (6.10), (6.11) we have precise agreement over a range of values of S provided that

$$b = 3\pi\lambda. \tag{6.12}$$

Thus, in $\mathcal{A}$ we have that

$$v_2(\mathbf{y}) = \frac{a}{s} + 3\pi\lambda - \frac{\lambda\sqrt{3}}{2} s.$$

The value of a is harder to estimate explicitly and for the present we simply assume that it has a similar magnitude to b.

Combining these expressions and rescaling, in an inner region for which $r = |\mathbf{x}|$ small, $s = \gamma^2 r$ large, we thus have

$$u(\mathbf{x}) = \frac{\gamma}{\sqrt{1 + \frac{\gamma^4 r^2}{3}}} + \left(\frac{a}{\gamma^2 r} + 3\pi\lambda - \frac{\lambda\sqrt{3}}{2} \gamma^2 r \right) + \mathcal{O}(1/\gamma^7). \tag{6.13}$$

6.1.2 The Outer Region

In an outer region which includes $\partial\Omega$ but excludes the origin, we set $u(\mathbf{x}) = t(\mathbf{x})/\gamma$ giving

$$\Delta t + \lambda t = -\frac{1}{\gamma^4} t^5 \qquad t|_{\partial\Omega} = 0. \tag{6.14}$$

As in the previous calculation we expand the function t as an asymptotic series of the form

$$t(\mathbf{x}) = t_1(\mathbf{x}) + \frac{1}{\gamma^4} t_2(\mathbf{x}) + \ldots.$$

Substituting this expression into (6.14) and considering terms of successive order we have

$$\begin{aligned} \Delta t_1 + \lambda t_1 &= 0 \qquad t_1|_{\partial\Omega} = 0 && (6.15)\\ \Delta t_2 + \lambda t_2 &= -t_1^5 \quad t_2|_{\partial\Omega} = 0 && (6.16) \end{aligned}$$

As remarked earlier, the solution of (6.15) which has a singularity at the origin is simply

$$t_1(\mathbf{x}) = AG_\lambda(\mathbf{x}, \mathbf{0}) = A \left(\frac{1}{4\pi|\mathbf{x}|} + g_\lambda(\mathbf{x}, \mathbf{0}) \right). \tag{6.17}$$

The expression (6.17) is a uniformly valid description of u in the outer region and we now consider the case of $|\mathbf{x}|$ small. For this range the dominant contribution to t_2 is given by solving

$$\Delta t_2 + \lambda t_2 = -(A/4\pi)^5 \frac{1}{r^5}$$

Now, making the assumption as before that for small r the dominant contribution to t_2 is radially symmetric we have

$$t_2 = -\frac{1}{6}(A/4\pi)^5 \frac{1}{r^3} + \mathcal{O}(1/r^5).$$

Thus combining these expressions and using (4.14) it follows that if r is small, the outer description of u is

$$u(\mathbf{x}) = \frac{A}{\gamma}\left[\frac{1}{4\pi r} + g_\lambda(\mathbf{0},\mathbf{0}) - \frac{\lambda}{8\pi} r\right] - \frac{1}{6\gamma^5}\left(\frac{A}{4\pi}\right)^5 \frac{1}{r^3}. \tag{6.18}$$

6.1.3 Matching

The two expressions (6.13) and (6.18) can be compared in the region $\mathcal{A}$ where r and u are small and s is large. From (6.13) we have

$$u = \frac{\sqrt{3}}{\gamma r} - \frac{3\sqrt{3}}{2\gamma^5 r^3} + \frac{a}{\gamma^5 r} + \frac{3\pi\lambda}{\gamma^3} - \frac{\lambda\sqrt{3} r}{2\gamma} + \mathcal{O}\left(\frac{1}{r^5}\right)$$

and from (6.18)

$$u = \frac{A}{4\pi\gamma r} + \frac{A}{\gamma} g_\lambda(0,0) - \frac{A\lambda r}{8\pi\gamma} - \frac{1}{6\gamma^5}\left(\frac{A}{4\pi}\right)^5 \frac{1}{r^3} \tag{6.19}$$

Considering firstly the non-constant terms, the two expressions agree for a range of values of r if

$$\frac{A}{4\pi\gamma} = \frac{\sqrt{3}}{\gamma} + \frac{a}{\gamma^5}, \quad \frac{1}{6\gamma^5}\left(\frac{A}{4\pi}\right)^5 = \frac{3\sqrt{3}}{2\gamma^5} \quad \text{and} \quad \frac{A\lambda}{8\pi\gamma} = \frac{\lambda\sqrt{3}}{2} \tag{6.20}$$

These expressions are all consistent to $\mathcal{O}(1/\gamma^4)$ if

$$A = 4\pi\sqrt{3} + \frac{4\pi a}{\gamma^4}. \tag{6.21}$$

In the calculations presented in Section 5, we found that with $\gamma = 8.812, \lambda = 7.5045$ that $A = 4\pi\sqrt{3} \times 1.0112$. This result is in excellent agreement with (6.21) and we estimate $a = 121$. For these values we also have $b = 70.6$ which gives support to our assumption that a and b have similar magnitudes.

Now considering the constant terms, we have agreement if

$$\frac{3\pi\lambda}{\gamma^2} = A g_\lambda(\mathbf{0},\mathbf{0}) + \mathcal{O}\left(\frac{1}{\gamma^4}\right),$$

so that

$$\gamma^{-2} = \frac{4}{\sqrt{3}\lambda} g_\lambda(\mathbf{0},\mathbf{0}) + O(1/\gamma^4). \tag{6.22}$$

which gives an asymptotic expression for γ. Now, as $\lambda \to \lambda_{**}$ then $g_\lambda(\mathbf{0},\mathbf{0}) \to 0$ and hence $\gamma \to \infty$. The asymptotic result (6.22) deduced from the numerical observation of the strong degree of radial symmetry of the peak and the close approximation of U_h to w_γ, is thus consistent with, and extends, McLeod's conjecture.

6.2 Asymptotics of the discrete solution for large γ

The formula (6.22) as a description of the continuous solution has been inferred from the results of computations, but appears inconsistent with the numerical computations as $\|U_h\|_\infty$ does not become unbounded. We now extend the asymptotic calculation to explain the discrepancy between the continuous and numerical results and to allow us to post-process the latter to obtain a more accurate solution.

The principle errors in the numerical approximation occurs when u is large and has a large gradient. This occurs at the peak, precisely when u is well approximated by w_γ with $\gamma = \|u\|_\infty$. Our computations have also shown that the discrete function U_h is close to w_γ if now $\gamma = \|U_h\|_\infty$. Thus we will proceed by calculating the difference between U_h and w_γ and using this calculation to estimate $\|U_h\|_\infty$. To obtain an asymptotic description of the piecewise linear function U_h we require a piecewise linear approximation of w_γ. A convenient such function is the interpolant $W_{\gamma,h}(\mathbf{x})$ to $w_\gamma(\mathbf{x})$ which is the piecewise linear function coinciding with $w_\gamma(\mathbf{x})$ on the nodes of the mesh. Provided that H is small the functions w_γ and $W_{\gamma,h}$ are close. As before, we consider a representation of the function $U_h(\mathbf{x})$ on an inner and an outer region.

6.2.1 The inner region

We rescale the functions so that $U_h(\mathbf{x}) = \gamma V_H(\gamma^2 \mathbf{x})$ and define $W_{\gamma,h}(\mathbf{x}) = \gamma W_{1,H}(\gamma^2\mathbf{x})$ where now $W_{1,H}(\mathbf{y})$ is the piecewise linear interpolant of the function $w_1(\mathbf{y})$ on a uniform mesh of size H. As before, we express the function $V_H(\mathbf{y})$ in an asymptotic series so that

$$V_H(\mathbf{y}) = V_{1,H}(\mathbf{y}) + \gamma^{-4} V_{2,H}(\mathbf{y}) + \ldots$$

By construction, for each basis function $\varphi_i(\mathbf{x}) \in S_h$, we have the identity

$$-a(U_h, \varphi_i) + \lambda\langle U_h, \varphi_i\rangle + \langle U_h^5, \varphi_i\rangle = 0.$$

Now suppose that $\varphi_{i,H}(\mathbf{y})$ is defined to be $\varphi_i(\mathbf{x})$ expressed on the rescaled mesh, and that all quadratures are now calculated with respect to $\mathbf{y}$. We have

$$-a(V_H, \varphi_{i,H}) + \frac{\lambda}{\gamma^4}\langle V_H, \varphi_{i,H}\rangle + \langle V_H^5, \varphi_{i,H}\rangle = 0.$$

Substituting the asymptotic expression for V_H into the above, gives equations for $V_{1,H}, V_{2,H}$ etc. For $V_{1,H}$ to satisfy the leading order equation exactly we would require

$$-a(V_{1,H}, \varphi_{i,H}) + \langle V_{1,H}^5, \varphi_{i,H}\rangle = 0. \tag{6.23}$$

In fact, (6.23) has the solution $w_1(\mathbf{y})$, but this function is not piecewise linear. Instead we take $V_{1,H}$ to be the interpolant $W_{1,H}$ and introduce a small discretisation error into the leading order expression, which enters into the calculation of the function $V_{2,H}$. This error can be expressed in terms of a residual R_i where

$$R_i \equiv -a(W_{1,H}, \varphi_{i,H}) + \langle W_{1,H}^5, \varphi_{i,H}\rangle.$$

Subtracting the identity (6.23) satisfied by w_1 gives

$$R_i = -a(W_{1,H} - w_1, \varphi_{i,H}) + \langle W_{1,H}^5 - w_1^5, \varphi_{i,H}\rangle. \tag{6.24}$$

Now looking at the next term in the asymptotic expansion for V_H and using (6.24) we have

$$-a(V_{2,H},\varphi_{i,H}) + 5\langle W_{1,H}^4 V_{2,H},\varphi_{i,H}\rangle = -\lambda\langle W_{1,H},\varphi_{i,H}\rangle + \gamma^4 R_i \tag{6.25}$$

If (6.3) is multiplied by $\varphi_{i,H}$ and integrated then a similar expression to (6.25) results, however, (6.25) has the additional term $\gamma^4 R_i$ due to the effect of the numerical discretisation. As $w_1(\mathbf{y})$ is a smooth function of $\mathbf{y}$ and, for small H, the function w_1 is closely approximated by its interpolant $W_{1,H}$, we can use results from interpolation theory to estimate the magnitude of R_i. In particular we use the following result.

Lemma 6.1 *Let $u(\mathbf{x}) \in C^4(\Omega)$ be an arbitrary function of $\mathbf{x} \in \mathbb{R}^3$, U_H its piecewise linear interpolant on a uniform mesh of size H and $f(u)$ a differentiable function of u. Now, consider an element $\mathcal{E}$ comprising eight adjacent cubes, each of side H centred on the origin $\mathbf{x} \equiv (x,y,z) = (0,0,0)$ with*

$$\varphi_H(\mathbf{x}) = (1-|x|/H)(1-|y|/H)(1-|z|/H) \quad \mathbf{x}\in\mathcal{E}, \quad \varphi_H(\mathbf{x}) = 0 \text{ otherwise}$$

the standard basis function on this element. Then, there are constants K_1 and K_2 independent of u and H, such that if H is sufficiently small then

$$R \equiv -a(u-U_H,\varphi) + \langle f(u) - f(U_H),\varphi\rangle = H^5(A+B) + O(H^7) \tag{6.26}$$

where

$$|A| < K_1 \max_{\mathcal{E}}\{|u_{xxyy}| + |u_{zzyy}| + |u_{xxzz}| + |u_{xxxx}| + |u_{yyyy}| + |u_{zzzz}|\} \tag{6.27}$$

and

$$|B| < K_2 \max_{\mathcal{E}}\{|f_u(u)|(|u_{xx}| + |u_{yy}| + |u_{zz}|)\}. \tag{6.28}$$

Proof. Suppose firstly that $a_{\mathcal{E}} \equiv a(u-U_H,\varphi_H) = ax + ay + az$ where

$$ax = \int_{z=-H}^{H}\int_{y=-H}^{H}\int_{x=-H}^{H}(u_x - U_{H,x})\varphi_{H,x}\,dxdydz \tag{6.29}$$

with similar expressions for ay and az. Using the expression for $\varphi_H(\mathbf{x})$ and integrating (6.29) we have

$$\begin{aligned} ax &= \frac{1}{H}\int_{z=-H}^{H}\int_{y=-H}^{H}\left([u-U_H]_{-H}^{0} - [u-U_H]_0^H\right)(1-|y|/H)(1-|z|/H)dydz \\ &= -\frac{1}{H}\int_{z=-H}^{H}\int_{y=-H}^{H}((u(H,y,z)-U_H(H,y,z)) - 2(u(0,y,z)-U_H(0,y,z)) \\ &\quad + (u(-H,y,z)-U_H(-H,y,z)))(1-|y|/H)(1-|z|/H)dydz. \end{aligned} \tag{6.30}$$

By the uniqueness and linearity of interpolation, it follows that if u is an odd function of y or of z then so is U_H. In the identity (6.30) the integration of all such odd functions vanishes. Thus we presume that the functions $u(H,y,z)$ etc. are even in y and z so that locally, the function u has the expansion

$$u(x,y,z) = p(x) + q(x)y^2 + r(x)z^2 + s(x)y^4 + t(x)y^2z^2 + n(x)z^4 + \text{h.o.t.}$$

where

$$p(x) = u(x,0,0), \quad q(x) = \frac{1}{2}u_{yy}(x,0,0), \quad r = \frac{1}{2}u_{zz}(x,0,0)$$

and $s(x) = \frac{1}{24} u_{yyyy}(x,0,0)$ etc. Now fix $x = H$ and consider the square $0 \leqslant y, z \leqslant H$. In this square we have

$$u(H,0,0) = p(H) \quad u(H,H,0) = p(H) + q(H)H^2 + \mathcal{O}(H^4),$$

$$u(H,0,H) = p(H) + r(H)H^2 + \mathcal{O}(H^4), \quad u(H,H,H) = p(H) + q(H)H^2 + r(H)H^2 + \mathcal{O}(H^4),$$

where the implied constant in the order H^4 terms is bounded by a multiple of $(|u_{yyyy}| + |u_{yyzz}| + |u_{zzzz}| + \mathcal{O}(H^2))$. From these point values we can calculate U_H. This then gives

$$u(H,y,z) = p(H) + q(H)y^2 + r(H)z^2 + \mathcal{O}(H^4),$$

$$U_H(H,y,z) = p(H) + q(H)Hy + r(H)Hz + \mathcal{O}(H^4),$$

so that

$$u(H,y,z) - U_H(H,y,z) = q(H)y(y-H) + r(H)z(z-H) + \mathcal{O}(H^4).$$

Similar expressions apply when $0 \leqslant y, z \leqslant H$ and $x = 0$ or $x = -H$. Thus, over the set $0 \leqslant y, z \leqslant H$ the contribution to the integral in (6.30) is given by

$$-\frac{1}{2H} \int_0^H \int_0^H [y(y-H)\,(u_{yy}(H,0,0) - 2u_{yy}(0,0,0) + u_{yy}(-H,0,0))$$

$$+z(z-H)\,(u_{zz}(H,0,0) - 2u_{zz}(0,0,0) + u_{zz}(-H,0,0)) + \mathcal{O}(H^4)](1 - y/H)(1 - z/H)dydz$$

$$= -\frac{1}{2H} \int_0^H \int_0^H [y(y-H)\,(H^2 u_{yyxx}(0,0,0) + \mathcal{O}(H^4))$$

$$+z(z-H)\,(H^2 u_{zzxx}(0,0,0) + \mathcal{O}(H^4)) + \mathcal{O}(H^4)](1 - y/H)(1 - z/H)dydz$$

$$= \mathcal{O}(H^5).$$

Here the implied constant in the order term is bounded by a multiple of $(|u_{yyxx}| + |u_{zzxx}| + |u_{yyyy}| + |u_{yyzz}| + |u_{zzzz}| + \mathcal{O}(H^2))$. Repeating this argument for the different ranges of y and z and then for ay and az gives (6.27).

Now, let $b_{\mathcal{E}} = |\langle f(u) - f(U_H), \varphi_H \rangle|$. As u and U_H are close if H is small, we can estimate this by $b \leqslant \max_{\mathcal{E}}\{|f_u(u)|\}\{|u - U_H|\}\langle 1, \varphi_H \rangle$. Now, standard results from interpolation theory imply that there is a constant K independent of u such that

$$\max_{\mathcal{E}}\{|u - U_H|\} < KH^2 \max_{\mathcal{E}}\{|u_{xx}| + |u_{yy}| + |u_{zz}|\}.$$

As $\langle 1, \varphi_H \rangle < 4H^3$, this gives $b_{\mathcal{E}} < H^5 B$ with B defined in (6.28).

Combining these expressions gives the result in the lemma. □

To apply this result to calculate R_i , we simply take $u = w_1, f(u) = u^5$ and note that the choice of the origin as being the centre of the element was quite arbitrary.

Now we consider again the equation (6.25). For large $s = |\mathbf{y}|$, $w_1(\mathbf{y}) \approx \sqrt{3}/s$ so that $\langle W_{1,H}, \varphi_{i,H} \rangle = \mathcal{O}(H^3/s)$. Now, the second derivatives of w_1 vary as $1/s^3$ and the fourth derivatives as $1/s^5$. Suppose that we look at the value of R_i corresponding to an element centred on $\mathbf{y}$. We can thus estimate that the corresponding values of A_i and B_i from (6.27),(6.28) to be

$$A_i < \alpha/|\mathbf{y}|^5, \quad B_i < \beta/|\mathbf{y}|^7 \tag{6.31}$$

where α and β are bounded independently of i. For this range we have $\langle W_{1,H}, \varphi_{i,H}\rangle \gg R_i$ provided that $H^3/s \gg \gamma^4 H^5/s^5$ which is satisfied if $s^4 \gg \gamma^4 H^2$ i.e. if $r \gg h$. Assuming this is the case (consistently with our numerical observations) we have that to a very good approximation

$$-a(V_{2,H}, \varphi_{i,H}) = -\langle \lambda\sqrt{3}/s, \varphi_{i,H}\rangle.$$

This equation is precisely the weak form of (6.4), in the range of $\mathbf{y}$ for which the resulting solution (6.5) is both smooth and has small second derivative terms proportional to $1/s^3$. The discrete solution is consequently a perturbation of the solution of (6.4) discretisation error proportional to H^2/s^3. Hence, there are constants a_H, b_H such that

$$V_{2,H}(\mathbf{y}) = \left(\frac{a_H}{|\mathbf{y}|} + b_H - \frac{\lambda\sqrt{3}|\mathbf{y}|}{2}\right)(1 + \mathcal{O}(H^2/|s|^2)) \tag{6.32}$$

We note that there is no *a priori* reason why b_H should equal b. In fact they differ by an amount proportional to $\gamma^4 H^2$.

We again use quadrature to estimate the value of the constant b_H. Suppose that $\Psi_H(\mathbf{y})$ is the piecewise linear interpolant to the function $\psi(\mathbf{y})$ defined in (6.6). Then differentiating (6.25) with respect to γ we have that for all i

$$-a(\Psi_H, \varphi_{i,H}) + \langle 5W_{1,H}^4 \Psi_H, \varphi_{i,H}\rangle = \gamma^3 T_i. \tag{6.33}$$

The exact expression for T_i is complex, but simple scaling arguments imply that there exists a constant C such that $|T_i| < C|R_i|$. (See the more detailed calculation given in [9].)

As in the calculation for the continuous case we exploit the close similarity between (6.33) and the expression (6.25) and employ a discrete form of the divergence theorem. Consider a cube $\mathcal{C} \subset \Omega_\gamma$ aligned with the mesh, centred on the origin and of side $2S$ where S is large and an integer multiple of H. Now introduce piecewise linear functions $\hat{\Psi}_H$ and $\hat{V}_{2,H}$ which coincide with Ψ_H and $V_{2,H}$ at all mesh points *interior* to $\mathcal{C}$, but which are zero on the boundary of, and exterior to, $\mathcal{C}$. As both the functions $\hat{\Psi}_H, \hat{V}_{2,H}$ are in the span of the set of functions $\varphi_{i,H}$, there exist V^i, Ψ^i such that

$$\hat{V}_{2,H} = \sum V^i \varphi_{i,H}, \quad \hat{\Psi}_H = \sum \Psi^i \varphi_{i,H}.$$

Taking a linear combination of (6.25) and (6.33) and subtracting gives

$$\begin{aligned} -a(V_{2,H}, \hat{\Psi}_H) + \langle 5W_{1,H}^4 V_{2,H}, \hat{\Psi}_H\rangle + a(\Psi_H, \hat{V}_{2,H}) - \langle 5W_{1,H}^4 \Psi_H, \hat{V}_{2,H}\rangle \\ = -\lambda\langle W_{1,H}, \hat{\Psi}\rangle + \gamma^4 \sum \Psi^i R_i(\mathbf{y}) - \gamma^3 \sum V^i T_i(\mathbf{y}). \end{aligned} \tag{6.34}$$

The left-hand side of (6.34) has two contributions given by

$$a(\Psi_H, \hat{V}_{2,H}) - a(V_{2,H}, \hat{\Psi}_H) \equiv a(\Psi_H - \hat{\Psi}_H, V_{2,H}) - a(V_{2,H} - \hat{V}_{2,H}, \Psi_H) \tag{6.35}$$

and

$$\begin{aligned} &5(\langle W_{1,H}^4 V_{2,H}, \hat{\Psi}_H\rangle - \langle W_{1,H}^4 \Psi_H, \hat{V}_{2,H}\rangle) \equiv \\ &\qquad 5(\langle W_{1,H}^4(\Psi_H - \hat{\Psi}_H), V_{2,H}\rangle - \langle W_{1,H}^4 (V_{2,H} - \hat{V}_{2,H}), \Psi_H\rangle). \end{aligned} \tag{6.36}$$

Both of these expressions only have contributions from integrals over those cubes adjacent to the boundary of $\mathcal{C}$. Furthermore, for large $\mathbf{y}$ the terms in expression (6.35) completely dominate those in (6.36) and we need only consider their contribution to (6.34). Consider (6.35) taking first the expression

$$a(\Psi_H - \hat{\Psi}_H, V_{2,H}). \tag{6.37}$$

For notational ease set $\chi = \Psi_H - \hat{\Psi}_H$ and $t = V_{2,H}$. Then if $-S < y, z < S$, we have $\chi(S - H, y, z) = 0$ and $\chi(S, y, z) = \Psi_H(S, y, z)$.

Consider now the face of $\mathcal{C}$ for which $x = S$ is constant. The contribution to (6.37) from integrals over cubes adjacent to this face is

$$\int_{y=-S}^{S} \int_{z=-S}^{S} \int_{x=S-H}^{S} (\chi_x t_x + \chi_y t_y + \chi_z t_z) dx dy dz.$$

As χ and t are piecewise linear functions, it follows that $\chi_x t_x$ does not depend upon x. Thus

$$\int_{x=S-H}^{S} \chi_x t_x dx = \Psi_H(S, y, z)(V_{2,H})_x(S, y, z) \tag{6.38}$$

where the derivative of $V_{2,H}$ is the value attained as x tends to S from below. Similarly, a direct calculation gives

$$\int_{x=S-H}^{S} \chi_y t_y dy dz = \frac{H}{6}(\Psi_H)_y(S, y, z)(2(V_{2,H})_y(S, y, z) + (V_{2,H})_y(S - H, y, z)), \tag{6.39}$$

with a similar result for $\chi_z t_z$. If we now consider the contribution over the same face of $\mathcal{C}$ of the second term $a(V_{2,H} - \hat{V}_{2,H}, \Psi_H)$ in (6.35) we obtain identical expressions to (6.38),(6.39) but with $V_{2,H}$ and Ψ_H interchanged. Subtracting the two expressions of the form (6.39) gives

$$\frac{H}{6}[((\Psi_H)_y(S - H, y, z)(V_{2,H})_y(S, y, z)) - (\Psi_H)_y(S, y, z)(V_{2,H})_y(S - H, y, z)] = \mathcal{O}(H^2).$$

Repeating this calculation over the faces $y = S$ and $z = S$ and combining these results, we obtain simply that

$$a(\Psi_H - \hat{\Psi}_H, V_{2,H}) - a(V_{2,H} - \hat{V}_{2,H}, \Psi_H) = \int_{\partial\mathcal{C}} (\Psi_H \nabla V_{2,H} - V_{2,H} \nabla \Psi_H).\mathbf{dA} + \mathcal{O}(H^2) \tag{6.40}$$

where $\mathbf{dA}$ is the surface area element of the cube with outward pointing normal, and the gradients are taken in an inner neighbourhood of the boundary.

Of most interest is the contribution to (6.40) by the term involving the constant b_H. This is simply

$$\int_{\partial\mathcal{C}} b_H \nabla \Psi_H.\mathbf{dA}$$

Now, from the explicit form of ψ we have for large $\mathbf{y}$ that $\nabla\Psi_H = \nabla\psi + \mathcal{O}(H/|\mathbf{y}|^3)$ and hence, evaluating the integral of $\nabla\psi$ over the cube explicitly, we have

$$\int_{\partial\mathcal{C}} b_H \nabla \Psi_H.\mathbf{dA} = 4\pi\sqrt{3} b_H(1 + \mathcal{O}(1/|\mathbf{y}|^2) + \mathcal{O}(H/|\mathbf{y}|)).$$

The other principle leading order contribution to (6.40) is then given by the surface integral of $-3\lambda\mathbf{y}/|\mathbf{y}|^2$ which evaluates explicitly to αS where

$$\alpha = -18\lambda \int_{-1}^{1} \arctan(1/\sqrt{1+t^2})/\sqrt{1+t^2} dt.$$

Now, returning to the expression (6.34) we then have, to leading order

$$4\pi\sqrt{3}b_H(1+\mathcal{O}(1/|\mathbf{y}|^2)+\mathcal{O}(H/|\mathbf{y}|b_H)+\alpha S=\sum\gamma^4\Psi_H^i R_i-\gamma^3 V^i T_i-\langle\lambda W_{1,H},\hat{\Psi}_H\rangle.$$

In the above, the inner product $\langle\lambda W_{1,H},\hat{\Psi}_H\rangle$ is the discrete form of the integral $\langle w_1,\psi\rangle$ over the cube. Again, this can be evaluated explicitly and for large S converges to $(\alpha S+12\pi\sqrt{3}\pi\lambda)(1+\mathcal{O}(H^2)$. Here, the constant implied in the $\mathcal{O}(H^2)$ term does not involve γ. Now consider the two sums which are taken over the elements interior to $\mathcal{C}$. As R_i decays rapidly for large $|\mathbf{y}|$, both sums rapidly tends toward a finite limit as S increases, thus we may take the sums to be infinite. This sum may be evaluated numerically by using the explicit construction for R_i over successively larger cubes and finer meshes. Note that as R_i and T_i scale as H^5 and the cube $\mathcal{C}$ contains $8S^3/H^3$ cubes of side H, the resulting sums scale as H^2. Numerical experiments confirm this relation. By making a series of calculations over successively finer meshes and for cubes of increasing size we estimate that

$$\sum_{i=1}^{\infty}\gamma^4\Psi_H^i R_i=-0.383184H^2\gamma^4+\mathcal{O}(H^3).$$

Now, the terms T_i each have similar magnitude to the terms R_i. Consequently, estimating $V_{2,H}$ by the dominant contribution of s we have that the sum involving T_i is at worst of order H^2 where the implied constant does not depend upon γ and this sum is thus dominated by the terms involving R_i.

By comparing constant terms in the expression for b_H we then have

$$b_H=-0.017605H^2\gamma^4+3\pi\lambda+\mathcal{O}(H^2), \tag{6.41}$$

and we see explicitly how b_H is a perturbation of the value of b calculated in (6.12).

We note that this estimate for b_H does *not* depend upon the domain, but does depend upon the fact that we are using cubes as elements. In principle we can also calculate b_H for other element shapes. In [9] a similar calculation of b_H for elements comprising concentric circles gave

$$b_H=-0.008863H^2\gamma^4+3\pi\lambda+\mathcal{O}(H^2).$$

Combining our estimates and rescaling we can derive an inner expression for U_H for r small and s large of the form

$$U_h=\gamma W_{1,H}(\gamma^2 x)+\gamma^{-3}\left(\frac{a}{\gamma^2|r|}+b_H-\frac{\lambda\sqrt{3}}{2}\gamma^2 r\right) \tag{6.42}$$

with b_H given by (6.41).

6.2.2 The Outer Region

The analysis in the outer region is much simpler as here the solution u is smooth and $U_h(\mathbf{x})$ is a good approximation. The error made in this approximation is proportional to h^2u'' and does not involve γ. The analysis then follows along similar lines as for the continuous case. Hence, we predict that as $|\mathbf{x}|$ is reduced

$$U_h(\mathbf{x})=\frac{\sqrt{3}}{\gamma}(1/|\mathbf{x}|+g_\lambda(\mathbf{x},\mathbf{0}))(1+\mathcal{O}(h^2/|\mathbf{x}|^2)), \tag{6.43}$$

where the error is small provided that $|\mathbf{x}|\gg h$. A more complete analysis of the error made in this expression for the closely related radially symmetric problem term is given in [9].

6.2.3 Matching

The two expressions (6.42) and (6.43) are very similar to the expressions for the continuous case, although the value of b is different. Following the analysis of the continuous case we have agreement provided that $b_H/\gamma^3 = 4\pi\sqrt{3}g_\lambda(\mathbf{0},\mathbf{0})/\gamma$. Substituting (6.41) into this relation and rescaling gives in the limit of large γ

$$\frac{-0.017605}{3\pi\lambda}h^2\gamma^6 + \gamma^{-2} = \frac{4}{\sqrt{3}\lambda}g_\lambda(\mathbf{0},\mathbf{0}) + \mathcal{O}(1/\gamma^4). \tag{6.44}$$

for those values of h for which $H \ll 1$.

The expression (6.44) extends the earlier expression (6.22) for $\|u\|_\infty$ to give an asymptotic description of the value of $\|U_h\|_\infty$. The most significant difference between these two expressions is that (6.44) is satisfied by a *finite* value of γ when $g_\lambda(\mathbf{0},\mathbf{0}) = 0$.

7 Conclusions from the Asymptotic Formulae

In this final section we now look at the predictions of the formula (6.44). We show that they are fully consistent with the numerical calculations. This gives support to the validity of the approach and also allows us to extrapolate the results to obtain a more accurate picture of the solution. These results can then be used as the basis of error estimates both for an adaptive mesh procedure and also for calculations on other domains.

7.1 Divergence for $\boldsymbol{\lambda = \lambda_{**}}$

For $\lambda \leqslant \lambda_{**}$ we have $g_\lambda(\mathbf{0},\mathbf{0}) \leqslant 0$. It is possible for the expression (6.44) to have solutions in this case, and these grow as h is reduced. This is fully consistent with the prediction of the existence of the spurious solutions. In particular, setting $\lambda = \lambda_{**}$ so that $g_\lambda(\mathbf{0},\mathbf{0}) = 0$ then for (6.44) to apply we must have

$$\gamma = \left(\frac{3\pi\lambda_{**}}{0.017605}\right)^{1/8} h^{-1/4} = 2.821h^{-1/4}, \tag{7.1}$$

giving (1.7). This result is in excellent agreement with the results presented in Table 5.2 of Section 5. The agreement is especially good when we consider that the calculated value of H when $h = 1/100$ is 0.774 which is not particularly small.

When $\lambda < \lambda_{**}$ the asymptotic formula predicts that γ grows like $h^{-1/4}$ for moderate values of γ and like $h^{-1/3}$ for larger values. Numerical experiments can only be made on feasible meshes for the moderate values and $\mathcal{O}(h^{-1/4})$ rates of growth are indeed observed in these cases.

7.2 Convergence for $\boldsymbol{\lambda > \lambda_{**}}$

If we substitute the formula (6.22) into (6.44) and set $\gamma = \|U_h\|_\infty, \Gamma = \|u\|_\infty$ we have to leading order

$$\frac{-0.017605}{3\pi\lambda}h^2\gamma^6 + \gamma^{-2} \approx \Gamma^{-2} \tag{7.2}$$

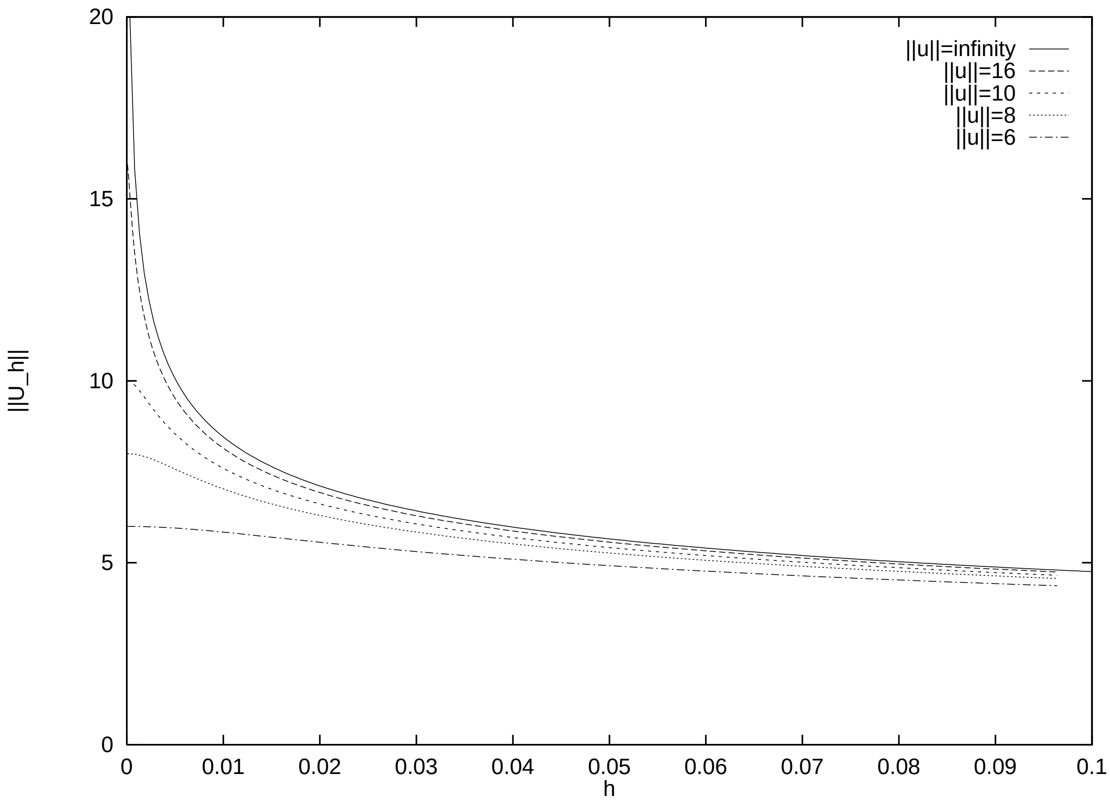

Figure 7.1: The value of $\|U_h\|_\infty$ as a function of h in the cases of $\|u\|_\infty = 6, 8, 10, 16, \infty$.

so that

$$\Gamma \approx \gamma / \sqrt{1 - Ch^2\gamma^8/\lambda}. \tag{7.3}$$

where $C = 0.0018679$ giving (1.6) in the introduction. In the limit of very small h we have

$$(\Gamma - \gamma)/\gamma = C\gamma^8 h^2/(2\lambda). \tag{7.4}$$

giving the result (1.5) in the introduction.

Observe that h has to be taken sufficiently small so that $h\gamma^4$ is small before the (standard) error estimate (7.4) is sharp. In fact the estimate (7.3) is descriptive over the wider range of values of h given by $h\gamma^2$ small. For values of h such that $h\gamma^2$ is small but $h\gamma^4$ is not small, the formula predicts that γ should again grow like $h^{-1/4}$ consistent with the results presented in Figure 5.3. It is of interest to compare the predictions of (7.3) with the results in Figure 5.3. Accordingly, we set $\lambda = \lambda_{**}$, take a sequence of values of $\Gamma = 6, 8, 10, 16, \infty$ (where the latter case is equivalent to using the formula (7.1)) and calculate γ as a function of h as h is reduced. This calculation gives the graph presented in Figure 7.1 which is directly comparable with Figure 5.3, and shows close similarity to it provided that h is sufficiently small.

To compare (7.3) more precisely with the calculated values, we consider the formula

$$\Gamma = \gamma / \sqrt{1 - Ch^2\gamma^8/\lambda}$$

to be exact for calculations on the two successive meshes given by $h = 1/90$ and $h = 1/100$ and use this to estimate C. The resulting estimates of C when λ is close to λ_{**} are then

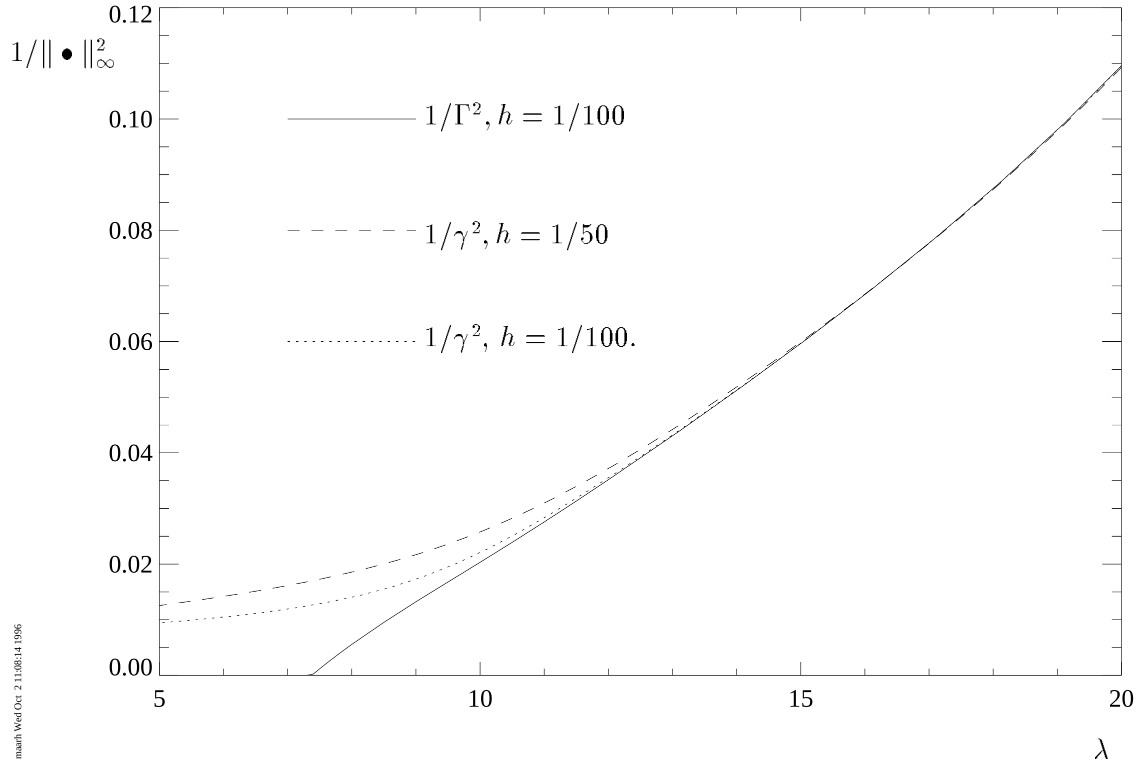

Figure 7.2: Graphs of $1/\|U_h\|_\infty^2$ for $h = 1/50$, $1/100$ together with the extrapolated value $1/\Gamma^2$ for $h = 1/100$ plotted against λ.

λ	C
7.5045	0.001531
8	0.001847
8.5	0.002168
9	0.002471
9.5	0.002783

These values are again in good agreement with the asymptotic formula - especially that given when $\lambda = 8$.

As a final calculation, we now use (7.3) to post-process the results. For a calculated value of γ on a mesh with $h = 1/100$ we determine the value of Γ given by (7.3). This extrapolated value serves as a better estimate for $\|u\|_\infty$ than γ. In Figure 7.2 we plot the resulting value of $1/\Gamma^2$ as a function of λ compared with the value of γ obtained when $h = 1/100$ and also when $h = 1/50$.

We now see that that the graph of $1/\Gamma^2$ is very close to being a straight line over a wide range of values of λ with an intercept very close to λ_{**}. This gives us further confidence in saying that $\lambda_0 = \lambda_{**}$.

The results from this discussion indicate how we should proceed to calculate on more complex domains and with finer meshes. Firstly, the result (7.3) involves a constant which depends upon the fact that we are using cubic elements but not on the precise domain used for the integration. Thus it can be used to post-process calculations on more complex domains. Secondly, the result (7.4) gives an asymptotic error estimate which can be incorporated into an adaptive mesh strategy. Some preliminary indications of the effectiveness of this are given in [8].

Acknowledgements

This work is part of an EPSRC funded research programme of joint investigations by Prof. Chris Budd and Drs. Tony Humphries and Andy Wathen into the theory and numerical analysis of nonlinear elliptic partial differential equations. We are also grateful to the EPSRC for their financial support through the grants GR/H63456 and GR/J75258.

References

[1] Adimurthi and S.L. Yadava. Elementary proof for the uniqueness of positive radial solution of a semilinear Dirichlet problem, 1992. Preprint.

[2] A. Bahri and J.M. Coron. On a nonlinear elliptic equation involving the criticl Sobolev exponent: The effect of the topology of the domain. *Comm. Pure. Appl. Math.*, 41:253–294, 1988.

[3] R.E. Bank. Analysis of a local a-posteriori error estimate for elliptic equations. In I. Babuska, O. Zienkiewicz, J. Gago, and E de Oliveira, editors, *Accuracy estimates and adaptive refinements in finite element computations*. Wiley, New York, 1986.

[4] H. Brezis. Elliptic equations with limiting Sobolev exponents – the impact of topology. *Comm. Pure Appl. Math.*, 39:S17–S39, 1986.

[5] H. Brezis and L. Nirenberg. Positive solutions of nonlinear elliptic equations involving critical Sobolev exponents. *Comm. Pure Appl. Math.*, 36:437–477, 1983.

[6] H. Brezis and L.A. Peletier. Asymptotics for elliptic equations involving critical growth. In *Partial Differential Equations and the Calculus of Variations, Volume I*, pages 149–192. Birkhäuser, 1989.

[7] C. Budd. Semilinear elliptic equations with near critical growth rates. *Proc. Roy. Soc. Edinburgh*, 107A:249–270, 1987.

[8] C.J. Budd and A.R. Humphries. Adaptive methods for semilinear elliptic equations with critical exponents and interior singularities. CMAIA Research Report 96/22, University of Sussex, 1996. Submitted to *Appl. Numer. Math.*

[9] C.J. Budd and A.R. Humphries. Weak finite dimensional approximations of radial solutions of semi-linear elliptic PDEs with near critical exponents. CMAIA Research Report 96/13, University of Sussex, 1996. Submitted to *J. Asymptotic Analysis.*

[10] C.J. Budd, A.R. Humphries, and A.J. Wathen. Finite element solutions for semi-linear elliptic PDEs on large 3D grids, 1996. In preparation.

[11] Y.S. Choi, P.J. McKenna, and M. Romano. A mountain pass method for the numerical solution of semilinear wave equations. *Numerische Mathematik*, 64:487–509, 1993.

[12] S.N. Chow and J.K. Hale. *Methods of Bifurcation Theory.* Springer-Verlag, New York, 1982.

[13] M. Crouziex and J. Rappaz. *On Numerical Approximation in Bifurcation Theory.* Springer-Verlag, New York, 1989.

[14] E.N. Dancer. The effect of domain shape on the number of positive solutions of certain nonlinear equations. *J. Diff. Eq.*, 74:120–156, 1988.

[15] M. Dobrowoloski and R. Rannacher. Finite element methods for nonlinear elliptic systems of second order. *Math. Nachr. Bd.*, 94:155–172, 1980.

[16] W-M. Gidas, B. Ni and L. Nirenberg. Symmetry and related properties via the maximum principle. *Comm. Math. Phys.*, 68:209–243, 1979.

[17] Zheng-Chao Han. Asymptotic approach to singular solutions for nonlinear elliptic equations involving critical Sobolev exponent. *Ann. Inst. Henri Poincaré*, 8:159–174, 1991.

[18] P.L. Lions. On the existence of positive solutions of semi-linear elliptic equations. *SIAM Review*, 24:441–467, 1982.

[19] J.C. Lopez-Marcos and J.M. Sanz-Serna. Stability and convergence in numerical analysis iii: Linear investigation of nonlinear stability. *IMA J. Num. Anal.*, 8:71–84, 1986.

[20] B. McLeod. A nonlinear elliptic equation with critical Sobolev exponent, 1984. Unpublished work.

[21] F. Merle, L.A. Peletier, and J. Serrin. A bifurcation problem at a singular limit. *Indiana University Math. J.*, 43:585–609, 1994.

[22] T. Murdoch and C.J. Budd. Convergent and spurious solutions of nonlinear elliptic equations. *IMA J. Numer. Anal.*, 12:365–386, 1992.

[23] S. Pohozaev. Eigenfunctions of the equation $\Delta u + \lambda f(u) = 0$. *Soviet Math. Dokl.*, 6:1408–1411, 1965. Translated from Dokl. Akad. Nauk SSSR 165, 1965, 33–36.

[24] O. Rey. Proof of two conjectures of H. Brezis and L.A. Peletier. *manuscripta math.*, 65:19–37, 1989.

[25] R. Schoen. Conformal deformation of a Riemannian metric to constant scalar curvature. *J. Diff. Geom.*, 20:479–495, 1984.

[26] A.M. Stuart and A.R. Humphries. *Dynamical Systems and Numerical Analysis.* Cambridge University Press, Cambridge, 1996.

[27] J.G. Verwer and R.A. Trompert. An adaptive-grid finite-difference method for time-dependent partial differential equations. In D. Griffiths and G. Watson, editors, *Numerical Analysis, 1991*, volume 260 of *Research Notes in Mathematics*. Pitman, 1992.

[28] S. Wang. The existence of a positive solution of semilinear elliptic equations with limiting Sobolev exponent. *Proc. Roy. Soc. Edinb.*, 117A:75–88, 1991.

[29] Juncheng. Wei. Locating the blow up point of a semilinear Direchlet problem involving critical Sobolev exponent, 1995. Preprint.